UNIVERSITAT POLITÈCNICA DE CATALUNYA

Departament de Física i Enginyeria Nuclear

ALEACIONES MOLECULARES BINARIAS EN FASE PLÁSTICA. ESTUDIO TERMODINÁMICO GLOBAL EN ALGUNOS DERIVADOS DEL NEOPENTANO.

Autor: Josep Salud Puig

Barcelona, gener de 1999

ANEXO I

La expresión de la entalpía molar de exceso de una disolución binaria dada por el modelo UBP, si X_1= 1-X y X_2= X, es de la forma:

$$H^E = N_o^2\left((1-X)\frac{a_{11}}{v_1} + X\frac{a_{22}}{v} - \frac{1}{v}\left((1-X)^2 a_{11} + 2(1-X)Xa_{ij} + X^2 a_{22}\right)\right) \qquad [A.1]$$

Por otra parte, el desarrollo de dicha función de acuerdo con un polinomio de Redlich-Kister de orden cuatro, se escribe como:

$$H^E = X(1\text{-}X)[H_1 + H_2(1\text{-}2X) + H_3(1\text{-}2X)^2 + H_4(1\text{-}2X)^3] \qquad [A.2]$$

Además, el volumen molar de la disolución, si se considera que V^E es nulo, se puede expresar como $v = (1\text{-}X)v_1 + Xv_2$. Teniendo en cuenta que $v_2 > v_1$ y, por tanto que $(v_2\text{-}v_1)/v_1 < 0$, se puede efectuar el siguiente desarrollo en serie de potencias:

$$\frac{1}{v} = \frac{1}{x(v_2 - v_1) + v_1} = \frac{1}{v_1}\frac{1}{1 + \frac{v_2 - v_1}{v_1}X} \cong$$

$$\frac{1}{v_1}\left(1 - \left(\frac{v_2 - v_1}{v_1}\right)X + \left(\frac{v_2 - v_1}{v_1}\right)^2 X^2 - \left(\frac{v_2 - v_1}{v_1}\right)^3 X^3 + \left(\frac{v_2 - v_1}{v_1}\right)^4 X^4 - ..\right) \qquad [A.3]$$

con la condición de ligadura:

$$\frac{1}{v(X=1)} = \frac{1}{v_2} \cong \frac{1}{v_1}\left(1 - \left(\frac{v_2 - v_1}{v_1}\right) + \left(\frac{v_2 - v_1}{v_1}\right)^2 - \left(\frac{v_2 - v_1}{v_1}\right)^3 + \left(\frac{v_2 - v_1}{v_1}\right)^4 - ..\right) \qquad [A.4]$$

para garantizar que [A.3] se convierta en $1/v_1$ para X = 0 y en $1/v_2$ para X = 1.

Dicha condición se puede comprobar que se cumple para valores cualesquiera de v_1 y v_2 si se toma un número de términos del desarrollo en $(v_2 - v_1)/v_1$ adecuado (con tres es suficiente para la mayoría de los casos).

Comparando los términos de cada uno de los polinomios que resultan de desarrollar [A.2] y [A.1] con la condición de ligadura [A.4], se obtienen las siguientes expresiones para los coeficientes H_1 y H_2:

$$H_1 = \frac{1}{v_1}\left[(a_{11} + a_{22} + 2a_{12}) + \left(\frac{a_{11}}{2} + a_{12} - \frac{3}{2}a_{22}\right)\left(\frac{v_2 - v_1}{v_1}\right) + \right.$$

$$\left(\frac{7a_{22}}{4} - \frac{a_{12}}{2} - \frac{a_{11}}{2}\right)\left(\frac{v_2 - v_1}{v_1}\right)^2 + \left(a_{11} - a_{22} - \frac{3a_{12}}{2}\right)\left(\frac{v_2 - v_1}{v_1}\right)^3 +$$

$$\left.\left(a_{22} + \frac{3a_{11}}{4}\right)\left(\frac{v_2 - v_1}{v_1}\right)^4 + \ldots.\right] \qquad [A.5]$$

$$H_2 = \frac{1}{v_1}\left[\left(\frac{v_2 - v_1}{v_1}\right)\left(\frac{a_{11} + a_{22}}{2} - a_{12}\right) + \left(\frac{v_2 - v_1}{v_1}\right)^2 (a_{12} - a_{22}) + \right.$$

$$\left.\left(\frac{v_2 - v_1}{v_1}\right)^3 \left(2a_{12} - \frac{3a_{11}}{2}\right) - \left(\frac{v_2 - v_1}{v_1}\right)^4 a_{11} + \ldots\right] \qquad [A.6]$$

donde sólo se han considerado los coeficientes H_1 y H_2 del desarrollo del polinomio de Redlich-Kister, puesto que únicamente tienen significado físico los dos primeros términos del desarrollo. No obstante, se ha utilizado un desarrollo de orden cuatro en la deduccción de las expresiones [A.5] y [A.6] para conseguir una mayor exactitud en la determinación de H_1 y H_2.

ANEXO II: La compacidad de algunos componentes de las series **I** y **III**.

En la Figura AII.1 se muestra la evolución del coeficiente de compacidad , en función de la temperatura, para algunos componentes de los sistemas binarios trataados en esta memoria. Asimismo, en la Tabla AII.1 se detallan los parámetros de los ajustes lineales de dicho coeficiente en función de la temperatura para cada compuesto.

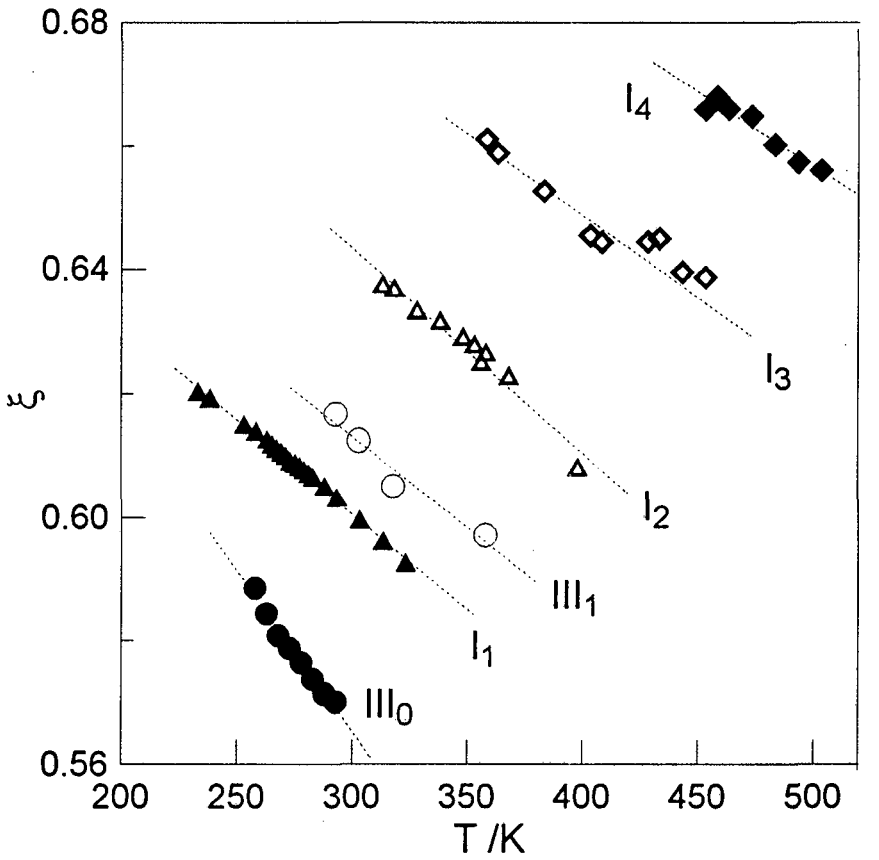

Figura AII.1. Evolución del coeficiente de compacidad para algunos compuestos de las series **I** y **III** con la temperatura.

Compuesto	$\xi = AT + B$	
	$Ax10^4$ (K^{-1})	B
$\mathbf{I_1}$	-3.0739	0.69264
$\mathbf{I_2}$	-3.2961	0.74221
$\mathbf{I_3}$	-2.6409	0.75432
$\mathbf{I_4}$	-2.4291	0.77809
$\mathbf{III_0}$	-5.2197	0.72184
$\mathbf{III_1}$	-2.9445	0.70137

Tabla AII.1. Parámetros de los ajustes lineales del coeficiente de compacidad en función de la temperatura para algunos componentes de las series **I** y **III**.

ANEXO III

Publicaciones relacionadas con el trabajo presentado en esta memoria:

1.- van Braak, J., López. D.O., Salud, J., Tamarit, J.Ll., Jacobs, M.H.G., Oonk, H.A.J., **The System Carbon Tetrabromide + Heachloroethane. Analysis of the Plastic-Crystalline + Liquid Equilibrium**. J. Cryst. Growth, 180; 315 (1997).

2.- Salud, J., López, D.O., Barrio, M., Tamarit, J.Ll., Oonk, H.A.J., Negrier, P., Haget, Y., **On the Crystallography and Thermodynamics in Orientationally Disordered Phases in Two-Component Systems**. J. Solid State Chem., 133; 536 (1997).

3.- Salud, J., Barrio, M., López, D.O., Tamarit, J.Ll., Alcobé, X., **Anisotropy of Intermolecular Interactions from the Study of the Thermal-Expansion Tensor**. J. Appl. Cryst., 31; 748 (1998).

4.- Salud, J., López, D.O., Barrio, M., Tamarit, J.Ll., **Two-Component Systems of Isomorphous Orientationally Disordered Crystals. Part I: Packing of the Mixed Crystals**. J. Mater. Chem. (sometido).

5.- Salud, J., López, D.O., Barrio, M., Tamarit, J.Ll., Oonk, H.A.J., **Two-Component Systems of Isomorphous Orientationally Disordered Crystals. Part II: Thermodynamic Analysis** J. Mater. Chem. (sometido).

ELSEVIER

Journal of Crystal Growth 180 (1997) 315–321

JOURNAL OF CRYSTAL GROWTH

The system carbon tetrabromide + hexachloroethane analysis of the plastic–crystalline + liquid equilibrium

J. van Braak[a], D.O. López[b], J. Salud[b], J.Ll. Tamarit[b], M.H.G. Jacobs[a,*], H.A.J. Oonk[a]

[a] *Petrology Group, Faculty of Earth Sciences, Utrecht University, Budapestlaan 4, 3584 CD Utrecht, The Netherlands*
[b] *Departament de Física i Enginyeria Nuclear, Universitat Politècnica de Catalunya, Diagonal 647, E-08028 Barcelona, Spain*

Received 18 March 1997

Abstract

A thermodynamic assessment was made of the (plastic–crystalline solid + liquid) phase diagram in the system carbon tetrabromide + hexachloroethane. The phase diagram is an example of crossed isodimorphism: two (plastic–crystalline solid + liquid) loops crossing each other give rise to a three-phase equilibrium (in this case eutectic). The information used consisted of experimental liquidus data, the thermodynamic melting properties of the pure components and the enthalpy of fusion data of the mixed plastic–crystalline solid state with the hexachloroethane structure. The eutectic is an organic analog for the investigation of eutectic growth in metallic systems. The eutectic temperature is 357.55 K and the calculated eutectic mole fractions are 0.094 (solid), 0.118 (liquid) and 0.187 (solid). The values of the initial distribution coefficients are (i) at the carbon tetrabromide side: $k_0^0 = 0.79 \pm 0.06$; (ii) at the hexachloroethane side: $k_0^0 = 0.58$.

PACS: 64; 64.60. – i; 64.60.My; 64.60.Dv; 64.70.Md; 64.75. + g; 65.50. + m; 82.60.Fa; 82.60.Hc; 82.60.Lf

Keywords: Thermodynamic optimization; Distribution coefficient; Orientationally disordered crystals; Eutectic growth; Carbon tetrabromide; Hexachloroethane

1. Introduction

In recent years the system {(1 − X) carbon tetrabromide + X hexachloroethane} has gained considerable interest. This is mainly due to the fact that its eutectic is a transparant model for the investigation of eutectic growth in nonfaceted lamellar structures. The coordinates of the eutectic three-phase equilibrium, in particular, play an important part in theoretical studies [1–6].

Before melting, carbon tetrabromide (CBr_4) as well as hexachloroethane (C_2Cl_6) have solid forms that are referred to as orientationally disordered crystals (ODIC) or plastic crystals. For that reason the binary system fits into our program of phase diagram analyses of binary systems having ODIC forms [7, 8]. In a wider context, pure substances and mixed systems which have ODIC forms are

* Corresponding author.

0022-0248/97/$17.00 Copyright © 1997 Elsevier Science B.V. All rights reserved
PII S0022-0248(97)00213-3

promising phase change materials for the storage of thermal energy and for thermal protection. For that reason they are the subject of experimental and theoretical studies of the Barcelona group [9, 10].

Solid carbon tetrabromide is known to occur in two different crystalline forms: II and α. The low-temperature form, II, is monoclinic with 32 molecules per unit cell (four independent molecules in the asymmetric unit) [11], the space group being C2/c [12, 13]. The high-temperature form, α, is an orientationally disordered fcc structure, with four molecules per unit cell [14, 15], which remains stable up to the melting point.

Solid hexachloroethane is known to occur in three different crystalline forms: III, II and β. The low-temperature form, III, is triclinic and stable up to 318 K. Form II is monoclinic. The high-temperature form, β (stable between 344 K and the melting point), is an ODIC form having a bcc structure [16, 17].

The binary phase diagram, as far as the transition from liquid to plastic crystalline solid is concerned, was determined in 1984 by Kaukler and Rutter [2]. More recently, Mergy et al. [4] studied the equilibrium relationships around the eutectic three-phase equilibrium. The main difference between the two sets of data is in the compositions of the solid phases at the three-phase equilibrium. The fact that the difference in composition of the two solid phases is a leading system dependent parameter in crystal growth studies, has been an extra stimulus to carry out the work presented in this paper.

The solid–liquid phase diagram of the CBr_4 + C_2Cl_6 system is an example of crossed isodimorphism [18]. Its two-phase region involving two solid phases and hence the occurrence of the (eutectic) three-phase equilibrium, is due to the incompatibility of the solid forms of CBr_4 and C_2Cl_6 to give rise to a continuous series of mixed crystals. The phase diagram, in such a case, can be considered as the result of two interfering solid–liquid loops: one loop involving a complete series of mixed crystals having the 'α form' and the other a complete series having the 'β form'. Part of the analysis consists of finding the metastable ends of these loops: the metastable melting points of the two pure components. In this respect the phase diagram is completely analogous to that of the system thianaphthene + naphthalene and the same holds true for its thermodynamic analysis [19, 20]. The analysis is based on the equal Gibbs energy curve (EGC) method [21] and is carried out, in part, with LIQFIT [22–24].

2. The plastic-crystalline solid–liquid equilibrium

2.1. Theoretical model

In order to describe all experimental information available for the binary system CBr_4 + C_2Cl_6, use has been made of the concept that the total Gibbs energy of the system is minimised when equilibrium is attained [21]. This concept is identical with assigning to each form a Gibbs energy function, from which all thermodynamic quantities of that form can be derived. The mixing properties of two substances in form φ are described with the following expression of the Gibbs energy:

$$G^{\varphi}(T, X_j) = \sum_{j=1}^{2} X_j \mu_j^{*\varphi}(T) + RT \sum_{j=1}^{2} X_j \ln (X_j) + G^{E\varphi}(T, X_j), \quad (1)$$

where X_j represents the mole fraction of component j in form φ, $\mu_j^{*\varphi}(T)$ the chemical potential of substance j in that form, R the gas constant and T the thermodynamic temperature. The first term on the right hand side of Eq. (1) represents the contribution to the Gibbs energy of the pure substances, the second term represents the ideal mixing term and the last term represents the deviation from ideal mixing between the substances. The latter term therefore is responsible for describing the interaction between the two different molecules. The excess Gibbs energy may be written in terms of excess enthalpy and excess entropy.

2.2. The hexachloroethane branch

The experimental information of this branch consists of liquidus, solidus and heat of fusion data from Kaukler and Rutter [2] and of two liquidus and two solidus points from Mergy et al. [4].

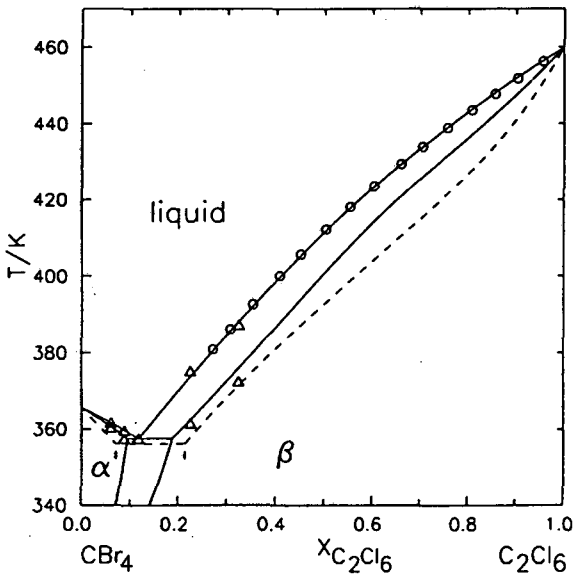

Fig. 1. Calculated and experimental phase diagram of carbon tetrabromide + hexachloroethane. ○: data points read off from the diagram given by Kaukler and Rutter [2]; △: data points of Mergy et al. [4]; - - -: Experimental phase diagram obtained by Kaukler and Rutter (the curves do *not* correspond to a thermodynamic analysis); —: calculated phase diagram.

Moreover all authors give the location of the three-phase equilibrium between the liquid-, α- and β phases.

An important feature in the thermodynamic assessment of the data is the determination of the metastable melting point of CBr_4 in the 'β form'. To establish this to an accurate extent, the liquidus data of Kaukler and Rutter [2] rather than their solidus data were used. The liquidus of the hexachloroethane branch of the phase diagram extends to a maximum of about 90% of the mole fraction scale, see Fig. 1. By extrapolating the liquidus to $X(CBr_4) = 0$ we obtained a value of 336.8 K for the metastable melting point.

In addition to phase diagram data, Kaukler and Rutter [2] provided information on the enthalpy of fusion as a function of composition. In fact, this information consists of data for the α to liquid transition (in the vicinity of pure CBr_4) in combination with data for the β to liquid transition (over a wide range of the composition scale); see Figs. 1 and 2. The extrapolation of these data to $X(CBr_4) = 0$, to obtain the enthalpy of fusion of CBr_4 in the metastable β-CBr_4 form, is rather arbitrary. Therefore we have included this enthalpy of fusion as a variable in the assessment. The enthalpy of fusion of C_2Cl_6 has been taken from a compilation given by Domalski and Hearing [25] and is 9749 J mol^{-1}.

Before carrying out the real assessment we decided to check the internal consistency of Kaukler and Rutter's [2] liquidus and solidus data using the program TXFIT [26]. From the analysis it appeared that the experimental solidus data cannot be reproduced within experimental error. Moreover, the analyses invariably showed that the reported composition of the β phase at the three-phase equilibrium is too high.

In view of these preliminary results we decided to use the liquidus data and heat of fusion data of Kaukler and Rutter [2] and the eutectic compositions of the liquid and β phase given by Mergy et al. [4] in the assessment using LIQFIT [22–24]. Assuming ideal mixing of the molecules in the liquid state, the variables in the analysis are the excess enthalpy and excess entropy of the 'β form' and heat of fusion of β-CBr_4 to liquid. The result is:

$$G^{E\beta}(T, X) = X(1 - X)[18291 - 45.88T/\mathrm{K} + (-3234 + 1.44T/\mathrm{K})(1 - 2X)]\ \mathrm{J\ mol^{-1}} \quad (2)$$

in which X denotes the mole fraction of C_2Cl_6. The assessed value for the enthalpy of fusion of CBr_4 is 6339 J mol^{-1}.

The stable part of the melting loop (β to liquid), calculated with the data in Table 1 and the excess Gibbs energy function given by Eq. (2), is part of the calculated phase diagram shown in Fig. 1. The maximum absolute difference between the temperature of input liquidus point and the calculated liquidus temperature is 0.3 K and the mean absolute difference is 0.19 K. The calculated heat of fusion of β-phase to liquid is compared with the experimental results of Kaukler and Rutter [2] in Fig. 2. The assessed value for the enthalpy of fusion of metastable β-CBr_4 (6339 J mol^{-1}) to liquid gives rise to a metastable transition of β-CBr_4 to α-CBr_4 at 309.44 K which is correctly lower than the transition of II-CBr_4 to α-CBr_4 (at 320 K [27]).

Table 1
The system carbon tetrabromide + hexachloroethane. Melting points and entropies of melting of the pure components (the metastable transition is denoted by superscript 'm', values for the concerned transitions have been calculated)

Substance	Transition	T_0/K	ΔS^*/(J K^{-1} mol^{-1})	Ref.
Hexachloroethane	$\beta \rightarrow$ liq	459.8	21.20	[2, 25]
Carbon tetrabromide	$\beta^m \rightarrow$ liq	336.8	18.82	Our work
Hexachloroethane	$\alpha^m \rightarrow$ liq	222.0	9.16	Our work
Carbon tetrabromide	$\alpha \rightarrow$ liq	365.65	9.16	[4]

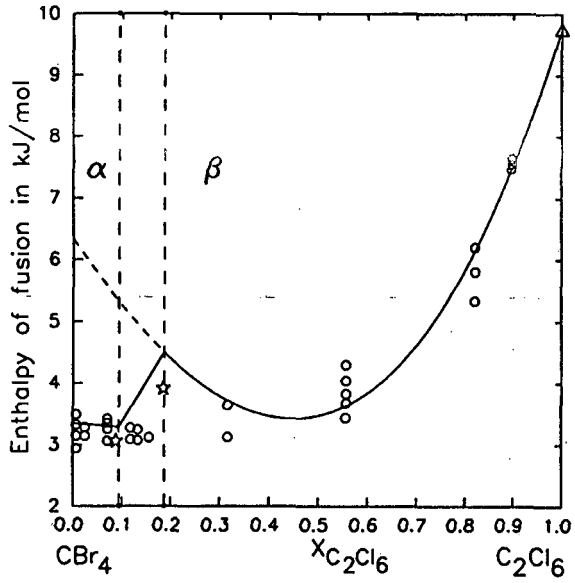

Fig. 2. Calculated enthalpy of fusion as a function of overall composition compared with the experimental data of (open circle) Kaukler and Rutter [2], (open triangle) extracted from a compilation of Domalsky and Hearing [25] and (open star) Mergy et al. [4]. Dashed curve represents the metastable extension. The vertical dashed lines indicate the eutectic compositions of the α and β phases.

2.3. The carbon tetrabromide branch

The stable part of the carbon tetrabromide branch extends over just about ten percent of the mole fraction scale. Accordingly, the information on which a thermodynamic analysis can be based is rather limited. Therefore we applied Van't Hoff's relation

$$\left(\frac{dX}{dT}\right)^{\alpha} - \left(\frac{dX}{dT}\right)^{Liq} = \frac{\Delta S_1^*}{RT_{01}} \qquad (3)$$

to the equilibrium between the α and liquid phases. In this relation ΔS_1^* represents the transition entropy and T_{01} the transition temperature of the first component. The use of this relation is justified because the phase equilibrium data for both the α phase as well as the liquid phase are located on straight lines connecting the melting point of CBr_4 and the positions given by the three-phase equilibrium within experimental error limits. Using the eutectic liquid composition (0.118 ± 0.006), eutectic temperature (357.55 ± 0.3) K and melting point of CBr_4 (365.65 ± 0.3) K, we calculate a eutectic composition of the α phase $X(C_2Cl_6) = (0.094 \pm 0.006)$. Comparing this result with the experimental value $X(C_2Cl_6) = (0.088 \pm 0.006)$ from Mergy et al. [4] it is concluded that the latter composition is shifted somewhat to the CBr_4 rich side of the phase diagram.

3. Discussion

3.1. The phase diagram and use of experimental data

For the analysis of the carbon tetrabromide branch of the phase diagram we preferred the data of Mergy et al. [4], which were determined with care by means of differential scanning calorimetry (DSC). They used small glass capsules in which the zone-refined and outgassed carbon tetrabromide is sealed under low argon pressure (to exclude a reaction with oxidizing agents). The DSC peak of such samples is reproducible and does not change by 24 h annealing at 393 K. For the final analysis of the hexachloroethane branch we only used the liquidus data by Kaukler and Rutter [2] and not the solidus data, because they prepared their mixed

Table 2
The system carbon tetrabromide + hexachloroethane. Calculated and reported location of the eutectic three-phase equilibrium

T_{eut}/K	X_α	X_{eut}	X_β	Ref.
357.15		0.117		[1]
356.15 (±0.1)	0.070	0.114 (±0.001)	0.213	[2]
357.55 (±0.3)	0.088 (±0.004)	0.118 (±0.006)	0.185 (±0.009)	[4]
357.55	0.094	0.118	0.187	This work

solid material in the calorimeter by quenching the tube in ice-water. It is known that such a procedure does not allow the determination of accurate solidus temperatures [28, 29]. This observation finds expression in the remaining disagreement between experimental data and calculated diagram. The maximum deviation between the calculated liquidus curve and the liquidus curve reported by Kaukler and Rutter [2] is 0.3 K which is far within their experimental error limits. The corresponding value for the solidus is 10 K.

The two reported liquidus points on the C_2Cl_6 branch from Mergy et al. [4] deviate 1.3 and 0.9 K from the calculated result. The corresponding two solidus points on this branche deviate 0.9 and 1.4 K from the calculated result.

The experimental liquidus data at the carbon tetrabromide side of the phase diagram from Mergy et al. [4] are reproduced within 0.09 K (mean deviation 0.05 K). Their reported solidus data are reproduced within 0.5 K.

The complete phase diagram is shown in Fig. 1, more precisely, the calculated stable part of it, along with the experimental data. The experimental and calculated coordinates of the eutectic three-phase equilibrium are displayed in Table 2. With the exception of X_α, the calculated mole fractions are, within experimental error, in agreement with the data given by Mergy et al. [4].

The calculated heat of fusion of the eutectic composition of the β phase (at $X(C_2Cl_6) = 0.187$) is 4503 J mol^{-1} which is in accordance with the value (3926 ± 157) J mol^{-1} given by Mergy et al. [4] considering the uncertainty in their eutectic composition. The calculated heat of fusion of the eutectic composition of the α phase (at $X(C_2Cl_6) = 0.094$) is 3284 J mol^{-1} which is in good agreement with the reported value (3071 ± 162) J mol^{-1} given by Mergy et al. [4].

3.2. The initial distribution coefficients

The equilibrium (superscript 0) distribution coefficient, k^0, is defined as (see Fig. 3)

$$k^0 = \frac{X_e^{sol}}{X_e^{liq}}, \tag{4}$$

where the subscript "e" indicates that the compositions are endpoints of tie lines. Its limiting value (subscript 0; $X_e^{Liq} \to 0$, $X_e^{Sol} \to 0$) is related to the thermodynamic properties as [21]

$$\ln k_0^0 = \frac{\Delta S_2^*(T_{02} - T_{01}) + (\partial \Delta G^E/\partial X)_{X\to 0}}{RT_{01}}. \tag{5}$$

The distinction between the CBr_4 and C_2Cl_6 branch is that T_{02} (the transition temperature of the second component) is known for the latter branch and unknown for the former branch. For the C_2Cl_6 branch it was therefore straightforward to derive a value for the transition entropy ΔS_2^* of the second component (which is CBr_4 in the application of Eq. (5)) and the difference excess Gibbs energy function between the liquid and β forms. The resulting value for k_0^0 is 0.580. The CBr_4 branch however, was described using Van't Hoff's relation which results in a value $k_0^0 = 0.79 \pm 0.06$ considering the experimental errors in the data. The latter value results in a wide range of possible values for both T_{02} and the first coefficient of the excess

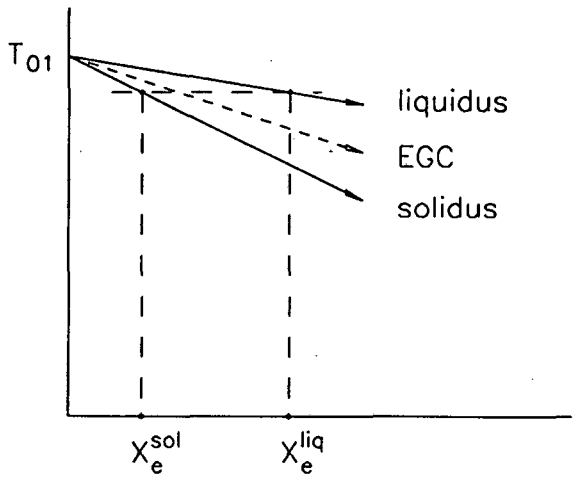

Fig. 3. The initial slope of the liquidus, solidus and equal Gibbs energy curve (EGC). The EGC is directly related to the difference excess Gibbs energy function (ΔG^E) of the liquid and solid phases [21].

Gibbs energy of the α phase. As an example we give

$$G^{E\alpha} = -682X(1-X)\ \mathrm{J\ mol^{-1}}, \quad (6)$$

where T_{02} and ΔS_2^* are given in Table 1.

3.3. The thermodynamic mixing properties

The single-phase region of the mixed crystalline state having the β form of hexachloroethane extends over a large part of the phase diagram. It implies that there is substantial information on the transition properties of the solid to liquid change. It is worthwhile to consider the physical significance of the data. From the position of the solid–liquid loop in the phase diagram it follows that for the transition the change in excess Gibbs energy, ΔG^E, is small. For the equimolar mixture we have, from Eq. (2),

$$\Delta G^E(X=0.5, T) = \Delta H^E(X=0.5) - T\,\Delta S^E(X=0.5) = (-4573 + 11.47\,T/\mathrm{K})\ \mathrm{J\ mol^{-1}}. \quad (7)$$

This result implies that the temperature θ of enthalpy–entropy compensation [30–32], the temperature at which ΔG^E passes zero, is $\theta = 399$ K. Incidentely, this θ is in the middle of the solid–liquid loop at $X = 0.5$. A comparable situation exists for the change from rotator form of solid to liquid in the case of a number of binary *n*-alkane systems for which $\theta = 320$ K [31].

Finally, it should be remarked that the calculated value of $\theta = 399$ K is rather independent of the lack of precision of ΔH^E. Therefore, it has real physical significance, as do have the initial distribution coefficients.

Acknowledgements

This is a Geodynamics Research Institute (Utrecht University) contribution 97.007. This project was supported by a DGYCIT grant, reference number PB-95-0032.

References

[1] K.A. Jackson, J.D. Hunt, Acta Metall. 13 (1965) 1212.
[2] W.F. Kaukler, J. Rutter, Mater. Sci. Eng. 65 (1984) L1.
[3] V. Seetharaman, R. Trivedi, Metall. Trans. 19 A (1988) 2955.
[4] J. Mergy, G. Faivre, C. Guthmann, R. Mellet, J. Crystal Growth 134 (1993) 353.
[5] P. Megnin, R. Trivedi, Acta Metall. Mater. 39 (1991) 453.
[6] Jincheng Liu, R. Elliott, J. Crystal Growth 148 (1995) 406.
[7] D.O. López, J. van Braak, J.Ll. Tamarit, H.A.J. Oonk, Calphad 18 (4) (1994) 387.
[8] D.O. López, J. van Braak, J.Ll. Tamarit, H.A.J. Oonk, Calphad 19 (1) (1994) 37.
[9] D.O. López, M. Barrio, J.Ll. Tamarit, P. Negrier, Y. Haget, Mol. Cryst. Liq. Cryst. 268 (1995) 129.
[10] M. Barrio, D.O. López, J.Ll. Tamarit, P. Negrier, Y. Haget, J. Solid State Chem. 124 (1996) 29.
[11] D. Michalski, M.A. White, J. Chem. Phys. 103 (14) (1995) 6173.
[12] C. Finbak, O. Hassel, Z. Phys. Chem. 36 (1937) 301.
[13] M. Moore, F. Baert, J. Lefebvre, Acta Crystallogr. B 33 (1977) 3681.
[14] M. Moore, J. Lefebvre, R. Fouret, Acta Crystallogr. B 33 (1977) 3682.
[15] M. Moore, J. Lefebvre, B. Hennion, B.M. Powel, C.M.E. Zeyen, J. Phys. Chem. 13 (1980) 2833.
[16] S. Seki, M. Momotani, Bull. Chem. Soc. Jpn. 23 (1) (1950) 30.
[17] W.J. Dunning, J. Phys. Chem. Solids 18 (1961) 21.
[18] F. Fried, L. Reinisch, J. Chim. Phys. 11 (1966) 1587.
[19] N. Klipp, P.R. van der Linde, H.A.J. Oonk, Calphad 15 (3) (1991) 235.

[20] H.A.J. Oonk, in: J.P. van der Eerden, O.S.L Bruinsma (Eds.), Science and Technology of Crystal Growth, Kluwer, Dordrecht, 1995, p. 27.
[21] H.A.J. Oonk, Phase Theory. The Thermodynamics of Heterogeneous Equilibria, Elsevier, Amsterdam, 1981.
[22] J.A. Bouwstra, A.C.G. van Genderen, N. Brouwer, H.A.J. Oonk, Thermochim. Acta 38 (1980) 97.
[23] J.A. Bouwstra, H.A.J. Oonk, Calphad 6 (1) (1982) 11.
[24] M.H.G. Jacobs, H.A.J. Oonk, LIQFIT, a computer program for the thermodynamic assessment of T-X liquidus or solidus data, Utrecht University, 1990.
[25] E.S. Domalski, E.D. Hearing, J. Phys. Chem. Ref. Data 19 (4) (1990) 890.
[26] M.H.G. Jacobs, H.A.J. Oonk, TXFIT, a computer program for the simultaneous thermodynamic assessment of T-X liquidus and solidus data, Utrecht University, 1990.
[27] R.S. Bradley, T. Drury, Trans. Faraday Soc. 55 (1959) 1844–1847.
[28] G.R. Atwood, Separation and Purification Methods 1 (1972) 297.
[29] P.R. van de Linde, Molecular mixed crystals from a thermodynamic point of view, thesis, Utrecht University, 1992.
[30] H.M.J. Boots, P.K. de Bokx, J. Phys. Chem. 93 (1989) 8240.
[31] W.J.M. van der Kemp, J.G. Blok, P.R. van der Linde, H.A.J. Oonk, A. Schuijff, M.L. Verdonk, Thermochim. Acta 225 (1993) 17.
[32] D. Mondieig, P. Espeau, L. Robles, Y. Haget, H.A.J. Oonk, M.A. Cuevas-Diarte, in preparation.

JOURNAL OF SOLID STATE CHEMISTRY 133, 536–544 (1997)
ARTICLE NO. SC977530

On the Crystallography and Thermodynamics in Orientationally Disordered Phases in Two-Component Systems

J. Salud,* D. O. López,* M. Barrio,* J. Ll. Tamarit,*,[1] H. A. J. Oonk,† P. Negrier,‡ and Y. Haget‡

*Departament de Física i Enginyeria Nuclear, Universitat Politècnica de Catalunya, ETSEIB,[2] Diagonal, 647, 08028 Barcelona, Catalonia, Spain;
†Petrology Group, Faculty of Earth Sciences,[2] Budapestlaan, 4, NL-3584 CD Utrecht, The Netherlands;
‡Laboratoire de Physique Moléculaire Optique et Hertzienne, URA 283 CNRS, Université Bordeaux I,[2] 351, Cours de la Libération, 33405 Talence, France

Received February 10, 1997; in revised form June 30, 1997; accepted June 30, 1997

The experimental two-component phase diagram between the orientationally disordered crystals 2-amino-2-methyl-1,3-propanediol (AMP) and 1,1,1-tris(hydroxymethyl)propane (PG) has been established from room temperature to the liquid state using thermal analysis and X-ray powder diffraction techniques. The intermolecular interactions in the orientationally disordered mixed crystals of the mentioned system and other related two-component systems are discussed by analyzing the evolution of the packing coefficient as a function of the the composition. A thermodynamic analysis of the presented phase diagram and the redetermined AMP/NPG (2,2-dimethyl-1,3-propanediol) is reported on the basis of the enthalpy–entropy compensation theory. © 1997 Academic Press

1. INTRODUCTION

Orientationally disordered crystals (ODICs) are molecular crystals characterized by high rotational mobility of molecules and low entropy of fusion (1). To understand the nature of the phases displaying such disorder, also called plastic phases, it is important to delve further into the molecular interactions that govern both structural and thermodynamic properties. To do so, several techniques have been applied to date to pure substances, such as NMR, neutron diffraction, and dielectric relaxation (2–4). Moreover, additional studies by means of techniques that are able to modify the intermolecular distances, such as high-pressure measurements, have been undertaken (5).

Another powerful way to modify the molecular surroundings is to introduce a foreign substance (6–8). In experimental practice this comes down to the study of binary systems. On this line of reasoning the present paper is devoted to the study of two binary systems of which the pure-component substances have ODICs. The systems are AMP/PG and AMP/NPG, where AMP = $NH_2(CH_3)C(CH_2OH)_2$, PG = $(CH_3)C(CH_2OH)_3$, and NPG = $(CH_3)_2C(CH_2OH)_2$. Because the ODIC form of AMP (body-centered cubic) is different from the ODIC form of the others (face-centered cubic), there are two types of molecular alloy. In terms of the phase diagrams this corresponds to the presence of two simple-(ODIC) phase fields separated by a two-phase region.

In this study the phase behaviour of the two systems is examined from the viewpoints of crystallography and thermodynamics. As for the aspect of crystallography special attention is given to the packing coefficient. With regard to the thermodynamic analysis a main part is devoted to the phenomenon of enthalpy–entropy compensation (9). Both packing coefficient and enthalpy–entropy compensation have become, in recent years, key issues in the study of mixed crystalline materials (10–14). The present paper underlines their importance and at the same time provides new experimental evidence.

2. EXPERIMENTAL

2.1. Materials

The substances were purchased from Aldrich Chemical Company with purities of 99.5% for AMP [2-amino-2-methyl-1,3-propanediol, $NH_2(CH_3)C(CH_2OH)_2$] and 99% for NPG [2,2-dimethyl, 1-3-propanediol, $(CH_3)_2C(CH_2OH)_2$] and PG[1,1,1-tris(hydroxymethyl)propane, $(CH_3)C(CH_2OH)_3$]. They were subjected to additional purification through repeated vacuum sublimation at 343, 353, and 393 K, respectively; the result was controlled by differential scanning calorimetry.

Two-component mixtures were prepared from the melt of the materials in the selected proportions by slow cooling to room temperature. The samples invariably were treated under a controlled Ar atmosphere.

[1]To whom correspondence should be addressed.
[2]All members of REALM.

0022-4596/97 $25.00
Copyright © 1997 by Academic Press
All rights of reproduction in any form reserved.

2.2. Diffraction at Constant Temperature

X-ray powder diffraction measurements were performed using a Siemens D-500 vertical diffractometer equipped with an Anton–Paar TTK temperature camera (± 0.5 K). The experimental conditions and the procedure have been described elsewhere (6, 15).

2.3. Diffraction as a Function of the Temperature

Powder diffraction measurements as a function of the continuous evolution of the temperature were made by means of a Guinier–Simon camera with Cu$K\alpha$ radiation, quartz monochromator, window width of 1 mm, film speed of 1 mm h^{-1}, and heating rates between 1 and 9 K h^{-1}. The powdered samples were sealed in Lindemann glass capillaries of 0.50-mm diameter.

2.4. Thermal Analysis

Thermal analysis was carried out by means of a Perkin–Elmer DSC-7 instrument, using a scanning rate of 2 K min^{-1} and ca. 5-mg sample masses hermetically sealed into aluminum crucibles under a controlled Ar atmosphere.

3. RESULTS

3.1. Polymorphism of the Pure Components

3.1.1. AMP $[NH_2(CH_3)C(CH_2OH)_2]$

The crystal structure of the low-temperature ordered form, phase II (hereafter denoted as M_1), is monoclinic with $Z = 4$ (16). Lattice parameters at 293 K are $a = 8.613(3)$ Å, $b = 11.037(4)$ Å, $c = 6.105(2)$ Å, and $b = 93.57(1)°$ (17). X-ray powder diffraction measurements at 313 K yielded the refined lattice parameters $a = 8.621(4)$ Å, $b = 11.053(5)$ Å, $c = 6.141(5)$ Å, and $\beta = 93.64(1)°$.

At 353.0 ± 1.0 K monoclinic AMP transforms into an orientationally disordered phase, the symmetry of which is body-centered cubic with $Z = 2$ (C_I). The latter phase is stable up to the melting at 384.7 ± 1.0 K. The cubic lattice parameter at 363 K has been determined to be 6.777(8) Å (17). The entropy changes for phase M_1-to-C_I and C_I-to-liquid transitions are 64.3 ± 1.8 and 7.0 ± 0.3 J K^{-1} mol^{-1}, respectively (18).

3.1.2. PG $[(CH_3)C(CH_2OH)_3]$

X-ray diffraction studies carried out on the ordered low temperature form (Q) between 293 and 393 K provided the lattice parameters for a tetragonal unit cell with space group $I\bar{4}$ and $Z = 2$ (19). The high temperature orientationally disordered form, which is stable between 356.6 ± 1.0 K and the melting point (473.7 ± 1.0 K), has face-centered cubic symmetry with $Z = 4$ (denoted as C_F) with a lattice parameter of 8.876(8) Å at 363 K (20, 21).

The entropy changes associated with the solid–solid transition and melting are 58.6 ± 5.0 and 10.0 ± 0.2 J K^{-1} mol^{-1}, respectively (18).

3.1.3. NPG $[(CH_3)_2C(CH_2OH)_2]$

The low-temperature form ($P2_1/c$, referred to as M_2) of NPG transforms at 314.3 ± 1.0 K to an orientationally disordered form, the symmetry of which is face-centered cubic (C_F) (22). The latter phase is stable to the melting point at 402.8 ± 1.0 K. Lattice parameters as well as thermodynamic data have been published elsewhere (23).

3.2. Two-Component Systems

3.2.1. AMP/PG Phase Diagram

3.2.1.1. Diffraction as a function of temperature. The Guinier–Simon patterns corresponding to the samples with PG mole fractions (X) of 0.40 and 0.55 together with those of the pure components AMP and PG are presented in Fig. 1.

For the sample with $X = 0.40$ the successive domains may be described as (i) the existence of a two-phase domain $[M_1 + Q]$; (ii) at ca. 321 K, disappearance of the reflections corresponding to the tetragonal Q phase and appearance of the cubic C_I phase giving rise to a $[M_1 + C_I]$ domain; (iii) at 330 K, disappearance of the M_1 phase. The $X = 0.55$ mixtures display the following features with increasing temperature: (i) transition from $[M_1 + Q]$ to $[Q + C_I]$ at ca. 321 K, (ii) disappearance of C_I and appearance of C_F at 326–328 K giving rise to a $[Q + C_F]$ two-phase domain; (iii) at higher temperatures, transformation of the $[Q + C_F]$ domain to a $[C_F]$ one-phase domain, i.e., to an orientationally disordered molecular alloy.

From the evidence displayed by the Guinier–Simon patterns it follows that there are two eutectoid invariants, $[M_1 + Q + C_I]$ and $[Q + C_I + C_F]$, at about 322 and 328 K, respectively. Owing to the small distance between the two invariants on the temperature scale, the instrument was set at the lowest possible scanning rate (1 K h^{-1}) and film speed (1 mm h^{-1}).

We were not able to make a proper registration of the transition from plastic crystalline solid to liquid. This has to do with large (differences in) vapor pressures which give rise to large concentration changes in the capillaries (at 390 K the equilibrium vapor pressures of pure AMP and PG are 72.77 and 11.10 Pa, respectively) (24).

3.2.1.2. Diffraction at constant temperature. This study was undertaken with two goals: first, to confirm the existence of the two detected close eutectoid invariants, and

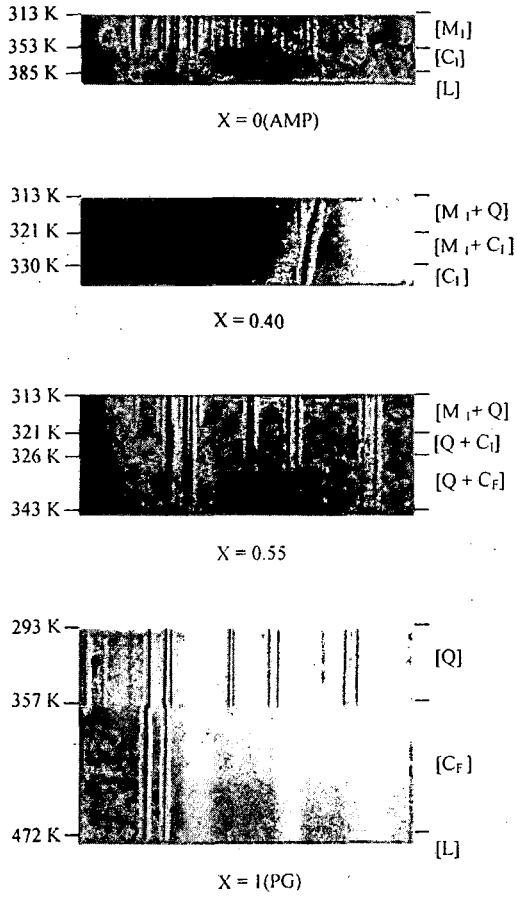

FIG. 1. Guinier–Simon patterns corresponding to the pure compounds AMP and PG and the samples $X = 0.40$ and $X = 0.55$.

second, to delimit the range of the $[M_1 + Q]$ and $[C_I + C_F]$ two-phase domains.

To verify the existence of the two invariants, several mixtures were studied at several temperatures. Figure 2

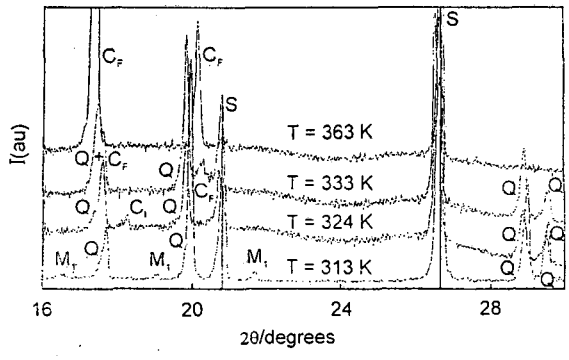

FIG. 2. 2θ window of the diffraction patterns for $X = 0.80$ at 313, 324, 333, and 363 K.

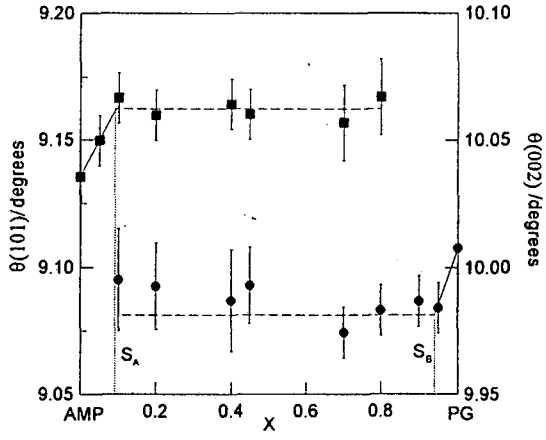

FIG. 3. Bragg angles, θ (degrees), as a function of the mole fraction (X) for the (101) (■) and (002) (●) reflections of the monoclinic and tetragonal lattices, respectively, at 313 K in the AMP/PG system.

shows a 2θ window of the diffraction patterns at 313, 324, 333, and 363 K. The successive domains $[M_1 + Q]$, $[Q + C_I]$, $[Q + C_F]$, and $[C_F]$ are clearly observed for a sample with a mole fraction of $X = 0.80$.

a. The solubility boundaries of the AMP and PG components at 313 K were established by studying the positions of the more intense reflections corresponding to the monoclinic M_1 and tetragonal Q lattices. Figure 3 depicts, as an example, the positions of the (101) and (002) reflections of the M and Q lattices, respectively, as a function of mole fraction. From the evolution of the angle positions of the reflections versus concentration, the solubility boundaries have been found to be S_A(313 K) $\cong$ 0.09, i.e., the molecular alloy $AMP_{0.91}PG_{0.09}$, and S_B(313 K) $\cong$ 0.96, i.e., $AMP_{0.04}PG_{0.96}$. Despite the small differences in the Bragg angles between the pure compounds and the average values of the samples belonging to the two-phase domain the lattice parameters of such limiting solid solutions were refined: $a = 8.633(4)$ Å, $b = 11.080(5)$ Å, $c = 6.112(5)$ Å, and $\beta = 93.61(1)°$ for the monoclinic solid solution, and $a = 6.055(2)$ Å and $c = 8.880(3)$ Å for the tetragonal one.

b. Figure 4 depicts the evolution of the Bragg angles of the (110) and (111) reflections corresponding to the bcc and fcc lattices at 363 K. Following the same procedure as in the previous case, the evolutions enabled us to establish the limits of the two-phase region between the two orientationally disordered single phase fields: S_A(363 K) $\cong$ 0.44 and S_B(363 K) $\cong$ 0.54.

The two-phase region between the two low-temperature forms and the one between the two high-temperature orientationally disordered phases are necessarily present owing to the nonisomorphous nature of the related phases. In addition it may be accented that the widths of the two types of two-phase regions are quite different: about 0.85 on the

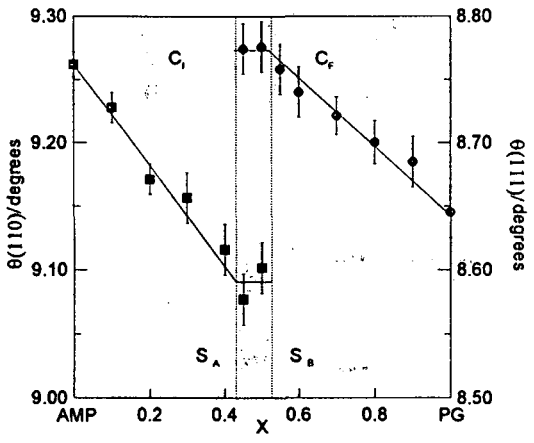

FIG. 4. Bragg angles, θ (degrees), as a function of the mole fraction (X) for the (110) (left side, ■) and (111) (right side, ●) reflections corresponding to the bcc and fcc lattices, respectively, at 363 K in the AMP/PG system.

mole fraction scale for the low-temperature form and about 0.10 for the high-temperature form. This experimental result is known to be the normal behavior of two-component systems of which the pure-component subtances have ODICs (10, 23).

3.2.1.3. Thermal Analysis. Accurate transition and melting temperatures were determined by means of thermal analysis, confirming the general trends observed by the diffraction studies.

The complete set of experimental data was used to construct the phase diagram represented by Fig. 5. The eutectoid invariants were set at 323.2 ± 1.0 K and 330.2 ± 1.5 K.

3.2.2. AMP/NPG Phase Diagram

Although the experimental AMP/NPG two-component system has been previously published by several authors (17, 25), a subsequent thermodynamic analysis has revealed some thermodynamic incoherences. These arise basically from the impossibility of accounting for the one- and two-phase low-temperature domains by means of the Gibbs energy functions calculated from the high-temperature equilibria. Disturbed by these incoherences we decided to redetermine the phase diagram, taking great care of the purity of the materials. The redetermined phase diagram, represented by Fig. 6, has the same global features as the one published earlier, but it has no more incoherences as shown below (Section 4.2). The temperatures of the (reestablished) eutectoid invariants are 293.7 ± 1.0 and 325.0 ± 1.2 K.

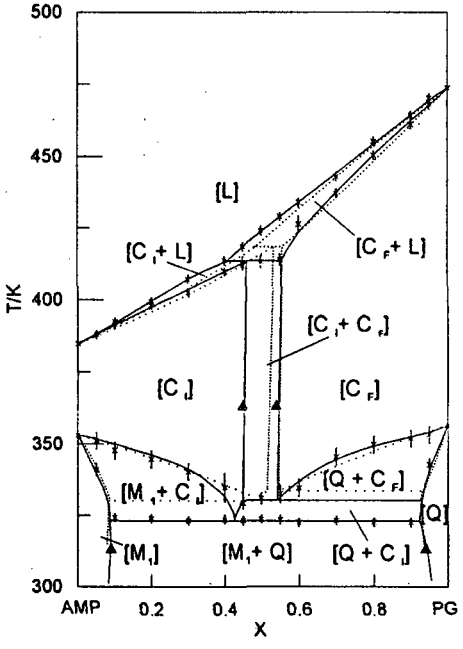

FIG. 5. Experimental and calculated (dotted line) phase diagrams of the the binary system AMP/PG: (×) DSC, (Δ) solubility boundaries determined by X-ray powder diffraction at constant temperature.

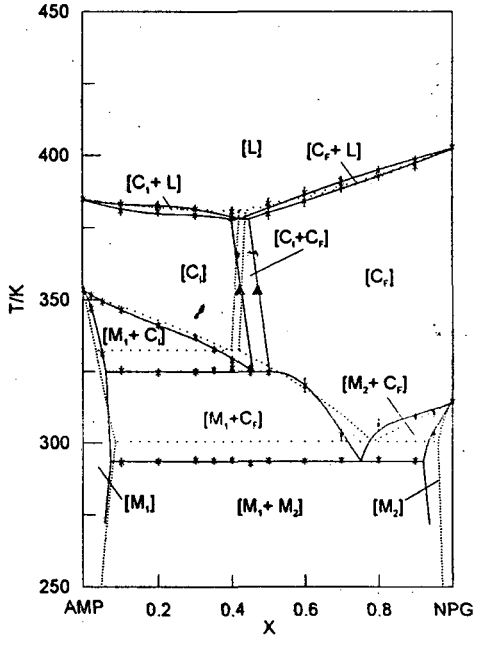

FIG. 6. Experimental and calculated (dotted line) phase diagrams of the binary system AMP/NPG: (×) DSC, (Δ) solubility boundaries determined by X-ray powder diffraction at constant temperature.

4. DISCUSSION

4.1. Intermolecular Interactions in the Disordered Molecular Alloys

In a recent paper, we showed that the intermolecular interactions by hydrogen bonds play an important role in the orientationally disordered phases (10). In particular, we extensively studied the molecular alloys formed between nonisomorphous plastic phases corresponding to some chemically and structurally related compounds formed by tetrahedral molecules belonging to two series $(CH_3)_{4-n}(CH_2OH)_n$, for $n = 1, \ldots, 4$ and $(NH_2)(CH_3)_{3-n}C(CH_2OH)_n$, for $n = 2$ and 3 (6, 17, 26). The compounds of the first series crystallize on cooling from the melt in a fcc lattice, whereas for those of the second series, the lattice corresponds to bcc symmetry. When mixing two compounds of the two different series, i.e., isomorphism is not displayed in the ODIC state, the intermolecular interactions by means of the hydrogen bonds control the packing of the mixed crystals in such a way that the packing coefficient of the molecular alloys (both bcc and fcc) increases with increasing number of CH_2OH and NH_2 groups in the average molecule of the alloy. Moreover, it was clearly shown by studying the PE/TRIS $[C(CH_2OH)_4/(NH_2)C(CH_2OH)_3]$ two-component system in the high-temperature disordered forms that the packing coefficient remains constant as a function of the molar fraction (6). This is to say that the strengths of the hydrogen bonds produced by the NH_2 group and those of the CH_2OH group become more or less equal in the disordered phases. To confirm the last assumption, the study of the packing coefficient evolution in the AMP/PG system is interesting, seeing that the total numbers of groups able to form hydrogen bonds in the considered molecules are equal: two CH_2OH groups and one NH_2 group in the AMP molecule and three CH_2OH groups in the PG molecule.

Considering the definition of packing coefficient, $\kappa(X) = V_m(X)/V_z(X)$, where V_m is the volume of an isolated molecule and V_z the volume of the crystal lattice per molecule, its calculation should be done by the experimental determination of V_z and by taking a model for the V_m value. The $V_z(X)$ values for the AMP/PG system can be straightforwardly calculated from the lattice parameter evolution, determined previously by means of X-ray powder diffraction at 363 K. The simplest way to calculate $V_m(X)$ is to set the average of the volumes of the isolated molecules participating in the alloy, i.e., the volume of the statistical entity,

$$V_m(X) = (1 - X)V_{mA} + XV_{mB}.$$

The volumes of the molecules considered have been calculated elsewhere [for details, see Refs. (10, 23)]. Figure 7 gives the evolution of the packing coefficient as a function of mole fraction for the two kinds of molecular alloy (bcc and fcc) and corresponding to the previously reported PE/Tris system (6) and for the AMP/PG system presented in this work. It is obvious that the packing parameter evolutions are almost flat for each kind of molecular alloy, showing that the substitution of the molecules does not produce any (perceptible) modification in the intermolecular interaction scheme. Moreover, we want to emphasize the relatively high values of the packing parameter for the pure compounds as well as for their alloys, which rules out incompatibility between high packing and the existence of orientational disorder (27).

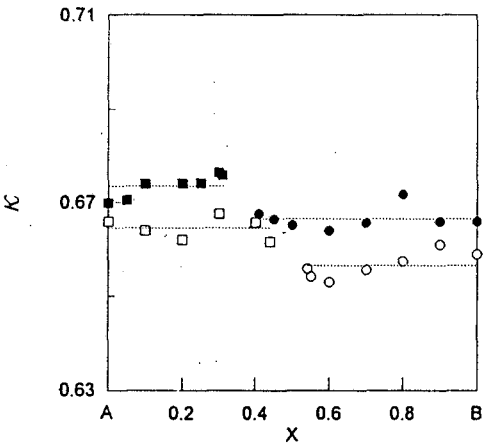

FIG. 7. Packing coefficient (κ) for the bcc (□, ■) and fcc (○, ●) molecular alloys corresponding to the two-component systems TRIS/PE (full symbols: ■, at 428 K; ● at 453 K) and AMP/PG (empty symbols: at 363 K).

4.2. Application of the Enthalpy–Entropy Compensation Theory

Under isobaric conditions, the thermodynamic properties of a binary system are known if for each of its forms the Gibbs energy of the pure substances is known as a function of temperature and the excess Gibbs energy of the mixture as a function of temperature and composition. The excess Gibbs energy, as any Gibbs energy, is composed of an enthalpy part and an entropy part,

$$G^E(T, X) = H^E(T, X) - T \cdot S^E(T, X), \qquad [1]$$

where X stands for mole fraction of the second component.

In the thermodynamic analysis that follows special attention is given to the phenomenon of enthalpy (H)–entropy (S) compensation (9, 12). The simplest way to formulate a compensation law is to define the excess Gibbs energy as a product of a temperature-dependent and system-independent factor $g(T)$ and a temperature-independent and

system-dependent factor $f(A_i)$, A_i being a collection of parameters describing a particular system of the class. In such a way, the excess Gibbs energy may be written

$$G^E(T, X) = g(T) \cdot f(A_i, X). \quad [2]$$

As the excess Gibbs energy must go through zero at the same temperature (T_c, the compensation temperature) for all the systems in the class, a suitable form for the $g(T)$ function is

$$g(T) = 1 - T/T_c. \quad [3]$$

With regard to $f(A_i, X)$ and taking into account the possible asymmetry on the concentration dependence of the excess Gibbs energy, the simplest $f(A_i, X)$ function may be defined as

$$f(A_i, X) = A_1 X(1 - X)\,[1 + A_2(1 - 2X)], \quad [4]$$

where A_1 and A_2 are the parameters that describe a particular system of a class. Moreover, it should be noted that the chosen form accounts directly for the magnitude (A_1) and for the asymmetry (A_2) of the excess Gibbs energy.

Inserting Eqs. [3] and [4] into Eq. (2) leads to the following expression for the excess Gibbs energy:

$$G^E(T, X) = (1 - T/T_c)\, A_1 X(1 - X)\,[1 + A_2(1 - 2X)]. \quad [5]$$

According to the selected formalism, the compensation temperature is the proportionality constant between excess enthalpy (H^E) and excess entropy (S^E), which follow from Eq. [5] as

$$H^E(T, X) = H^E(X) = A_1 X(1 - X)[1 + A_2(1 - 2X)] \quad [6a]$$

$$S^E(T, X) = S^E(X) = A_1 X(1 - X)[1 + A_2(1 - 2X)]/T_c. \quad [6b]$$

In the case of the two-component systems analyzed here, the components have different lattice symmetry in the orientationally disordered phases, either bcc or fcc, implying that they are nonisomorphous. Thus, each kind of solid solution will be described by means of an excess Gibbs energy of the form of [5] with different A_i parameters. The nonisomorphism of the disordered phases present gives rise to the existence of two different orientationally disordered liquid equilibrium loops in both of the considered phase diagrams. The metastable extensions of these loops end in the theoretical metastable melting points of the pure substances corresponding to a phase that is assumed to be isomorphous with the phase for which the extension of the loop is done. To estimate the fcc and bcc metastable melting points of the AMP and PG metastable phases, the narrow stable [C_F + L] and [C_I + L] branches in the AMP/PG system were extrapolated to $X = 1$ and $X = 0$, respectively, by means of a simple procedure in terms of the equal-Gibbs-curve (EGC) method (28, 29). The values of the metastable points determined are summarized in Table 1. The same procedure used to determine the metastable melting points provides the differences in the excess Gibbs energy functions between the disordered and liquid phases. Because not only differences in the excess Gibbs energies but also specific values of these functions are required to calculate the ordered–disordered phase equilibria, some assumptions have to be made about the excess properties of the liquid solution. In want of such values we have neglected the excess Gibbs energies of the liquid mixtures; thus the minus ΔG^E functions were identified with the G^E functions for the mixed orientationally disordered states.

To determine the temperature dependence of the G^E function, i.e., the value of the compensation temperature, the derived excess Gibbs energy data have to be combined with the excess enthalpy data. At a given temperature T, the relation

$$T_c = T/(1 - G^E(T, X)/H^E(X)) \quad [7]$$

can be directly derived from expressions [6a] and [5]. Exact excess enthalpy data are rather difficult to obtain. Nevertheless, the heat of melting as a function of the mol fraction for the AMP/PG system has been measured (see Fig. 8) in each solid solution domain. Assuming the temperature-independent excess enthalpy form of Eq. [6a] and according to the

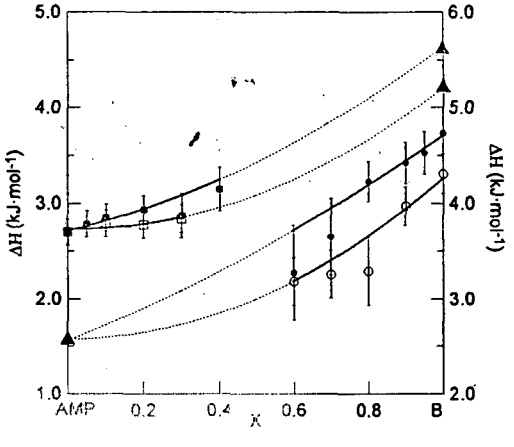

FIG. 8. Enthalpies of melting for the bcc (□, ■, right side) and fcc (○, ●, left side) molecular alloys corresponding to the two-component systems AMP/PG (B ≡ PG, full symbols) and AMP/NPG (B ≡ NPG, empty symbols). The triangles correspond to the calculated metastable values.

nonexistence of excess values for the liquid solution, the excess enthalpy for each solid solution was obtained by fitting a second-order polynomial to the experimental data displayed in Fig. 8. Combining the results for H^E and G^E, the value of $T_c \cong 800$ K is obtained for both bcc and fcc alloys in the AMP/PG system. The procedure used needs to fix the enthalpy of melting corresponding to metastable phases. These values were obtained by taking the entropy of melting to be the same as that of the stable form. The values obtained are included in Table 1.

Finally, the excess Gibbs energy and T_c values are used to determine the A_1 and A_2 parameters for the two orientationally disordered phases. These values are summarized in Table 1. It is important to note that, from a thermodynamic point of view, the temperature dependence is similar for both bcc and fcc molecular alloys in this AMP/PG system, as shown from the same value of temperature T_c. Similar findings, equal T_c temperature values for a large number of two-component systems of alkanes have been recently reported (30).

For the AMP/NPG phase diagram a more or less similar procedure was followed. In this case, taking notice of the close behavior of bcc and fcc molecular alloys in the previous analyzed system, we assume that the alloys of the AMP/NPG system have the same compensation temperature, i.e., $T_c = 800$ K. The system-dependent A_1 and A_2 parameters for each kind of solid solution in this system are collected in Table 1.

The miscibility in the ordered low-temperature forms of both AMP/PG and AMP/NPG systems is almost negligible (see Figs. 5 and 6, respectively), so then, the complete phase diagrams were calculated by using the excess Gibbs energies corresponding to the disordered high-temperature forms previously determined. The final resulting phase diagrams calculated by means of the ProPhase program (31) are shown in Figs. 5 and 6. Attempts to improve the agreement between calculated and experimental phase diagrams were performed by considering the limited miscibility in the ordered forms, but no noticeable improvements were reached.

Notwithstanding the difficulty of calculating the presented phase diagrams (due to the relatively poor experimental data and accessibility to some parameters needed to perform the thermodynamic analysis), our goal has been to find a compromise between physical significance and agreement between calculated and experimental phase diagrams for the orientationally disordered phases. From this point of view, the agreement can be considered as satisfactory (see Table 2) and the coherence of the model, i.e., the representation of the physical reality, can be considered valid. In Fig. 8 we show the experimental and the calculated enthalpies of melting for the bcc and fcc molecular alloys of the AMP/NPG system. It should be mentioned that in the calculation of this phase diagram the T_c value was assumed to be exactly the same as in the previous one (AMP/PG) by assuming that the two binary systems belong to the same class. So then, the experimental values of the excess enthalpy for the AMP/NPG system were considered, and notwithstanding, the agreement between calculated and experimental excess enthalpy values is satisfactory (see Fig. 8).

From a thermodynamic analysis point of view, the calculation problems can be divided into two types: (i) the determination of the metastable properties (as melting temperature and melting enthalpy) corresponding to the isomorphous metastable phases of the compounds which have to be considered to build up the needed crossed isodimorphism; (ii) the model itself used. With regard to this

TABLE 1

Temperatures and Enthalpies of Melting of the Stable (s) and Metastable (m) bcc and fcc Forms Together with the Calculated Values of the System-Dependent A_1 and A_2 Parameters of the Binary Systems AMP/PG and AMP/NPG

		AMP/PG	AMP/NPG
bcc	T_1 (K)	384.7 (s)	384.7 (s)
	T_2 (K)	465.0 (m)	393.1 (m)
	ΔH_1 (J mol^{-1})	2700 (s)	2700 (s)
	ΔH_2 (J mol^{-1})	4650 (m)	4206 (m)
	A_1 (J mol^{-1})	1003	584
	A_2	− 0.23	− 0.33
fcc	T_1 (K)	363.5 (m)	363.5 (m)
	T_2 (K)	473.7 (s)	402.8 (s)
	ΔH_1 (J mol^{-1})	2552 (m)	2552 (m)
	ΔH_2 (J mol^{-1})	4737 (s)	4310 (s)
	A_1 (J mol^{-1})	860	296
	A_2	0.06	− 1.33

TABLE 2

Comparison between Experimental (E) and Calculated (C) Invariant Equilibria

System	Invariant		T (K)	X_M	X_N	X_P
AMP/NPG	Eutectoid	E	293.7	0.05	0.75	0.92
		C	300.5	0.09	0.79	0.98
	Eutectoid	E	325.0	0.06	0.46	0.51
		C	332.5	0.04	0.40	0.42
	Eutectic	E	377.5	0.38	0.42	0.44
		C	380.8	0.41	0.42	0.43
AMP/PG	Eutectoid	E	323.0	0.09	0.43	0.92
		C	330.0	0.09	0.47	0.92
	Eutectoid	E	330.2	0.44	0.53	0.93
		C	333.5	0.51	0.54	0.96
	Peritectic	E	413.6	0.40	0.47	0.57
		C	418.4	0.48	0.53	0.56

fact, it can be seen that, for both phase diagrams, the most discordant results concern the two-phase regions between the two orientational single phase fields which produce a considerable difference between calculated and experimentally determined eutectic (case of the AMP/NPG) and peritectic (case of the AMP/PG) invariants, 3.3 and 5.3 K, respectively. Such discrepancies are basically produced by the selected form of the temperature-dependent system-independent factor $g(T)$. This choice, in addition to the temperature-independent excess enthalpy and entropy expressions, does not allow fitting of the two-phase regions, these being a direct consequence of the excess Gibbs energies determined from the orientationally disordered liquid phase equilibria.

An empirical estimation method for the enthalpy–entropy compensation temperature in terms of a quasi-subregular solution model including a compensation law was published (32). From the experimental evidence of a large variety of mixtures relating molecular mixtures (such as *p*-dihalobenzenes, alkali halides, alkaline earth oxides, and cryogenic noble gases), the equation

$$T_c = (4.0 \pm 0.16) T_1 T_2/(T_1 + T_2), \qquad [8]$$

in which T_1 and T_2 are the melting temperatures of the first and second components in the mixture, was derived. It should be mentioned that for all the mixtures used isomorphism was supposed to exist; i.e., one Gibbs energy curve was sufficient to describe the behavior of the solid solutions. This is not the case for the systems presented in this paper, so then, the empirical relation [8] must be used carefully. In particular, the enthalpy–entropy compensation temperature is associated with each solid solution domain, and then, expression [8] should be applied by using the stable and metastable temperatures of the solid solutions considered. If such a method is followed the T_c calculated by Eq. [8] are 842 and 778 K for the bcc alloys and 823 and 764 K for the fcc alloys for the AMP/PG and AMP/NPG systems, respectively. By averaging the calculated values, a temperature of 802 K is obtained, which is certainly close to the value calculated from the thermodynamic analysis performed (800 K). However, this excellent agreement may be circumstantial because Eq. [8] was obtained from thermodynamic analysis of solid–liquid equilibria where a large number of the molecular alloys did not display orientational disorder.

In a more general framework T_c values were calculated for a set of independent systems (14). From this study it follows that the enthalpy–entropy compensation temperature is above the melting range for each of the considered systems. Such experimental evidence was mathematically expressed by means of the quotient $\log T_c/\log T_{EGC}$ $(X = 0.5) = 1.10 \pm 0.05$, where $T_{EGC}(X = 0.5)$ represents the temperature of the equal-Gibbs curve at $X = 0.5$ (29). For some binary systems such as *l*-carvoxime + *d*-carvoxime, and gold + palladium, the quotient differs significantly from the rule (1.03 and 1.04, respectively). More recently, two sets of orientationally disordered mixed crystals were the subject of a similar thermodynamic analysis; for the first set, relating two-component systems displaying complete miscibility (33) (i.e., isomorphism being proved), the calculated quotient is about 1.09; however, for the second set (13), where the enclosed systems display crossed isodimorphism as in the systems of the present work, the quotient (about 0.97) differs from the mean by somewhat more than the standard deviation. At present, a still unpublished work (34) relating ODIC mixed crystals between CBr_4 and C_2Cl_6 compounds shows close behavior, more precisely, a quotient of 1.01. For the two-component systems determined in the present work the quotients, the accuracy of which is somewhat limited, can be considered as satisfactory due to the carefully performed thermodynamic analysis and are 1.12 and 1.11 for AMP/NPG and AMP/PG systems, respectively. It may be remarked that, from a macroscopic thermodynamic point of view, the model used is capable of giving a correct description of the phase diagrams and the thermodynamic properties of mixed crystals in the orientationally disordered state.

Further work has to be carried out to correlate the validity of the perhaps too simple assumed temperature function $g(T)$, as well as, in such a case, to verify the up to date experimental evidence of Eq. [8].

ACKNOWLEDGMENT

This work has been supported by the Spanish Dirección General de Investigación para la Ciencia y la Tecnología under Grant PB95-0032.

REFERENCES

1. J. Timmermans, *J. Phys. Chem. Solids* **18**, 1 (1961).
2. S. Urban, *Adv. Mol. Relax. Int. Proc.* **21**, 221 (1981).
3. J. N. Sherwood, "The Plastically-Crystalline State." Wiley, New York, 1979.
4. N. G. Parsonage and L. A. K. Staveley, "Disorder in Crystals." Clarendon, Oxford, 1978.
5. A. Würflinger, *Int. Rev. Phys. Chem.* **12**, 89 (1993).
6. M. Barrio, D. O. López, J. Ll. Tamarit, P. Negrier, and Y. Haget, *J. Solid State Chem.* **124**, 29 (1996).
7. M. N. Akimov, O. F. Bezrukov, O. V. Chikunov, and A. V. Struts, *J. Chem. Phys.* **95**(1), 22 (1991).
8. A. R. Britcher and J. H. Strange, *J. Chem. Phys.* **75**, 2029 (1981).
9. H. M. Boots and P. K. de Bokx, *J. Phys. Chem.* **93**, 8240 (1989).
10. J. Ll. Tamarit, M. Barrio, D. O. López, and Y. Haget, *J. Appl. Crystallogr.* **30**, 118 (1997).
11. T. Calvet, M. A. Cuevas-Diarte, H. E. Gallis, and H. A. J. Oonk, *Recl. Trav. Chim. Pays-Bas* **115**, 333 (1996).
12. W. J. M. van der Kemp, J. G. Blok, P. R. van der Linde, H. A. J. Oonk, A. Schuijff, and M. L. Verdonk, *Calphad* **18**, 255 (1994).
13. D. O. López, J. van Braak, J. Ll. Tamarit, and H. A. J. Oonk, *Calphad* **19**, 37 (1995).

14. H. A. J. Oonk, T. Calvet, W. J. M. van der Kemp, and M. L. Verdonk, *in* "XIXèmes Journées d'étude des equilibres entre phases" (M. A. Cuevas-Diarte, J. Ll. Tamarit, and E. Estop, Eds.), p. 355. Barcelona, 1993.
15. M. Barrio, J. Font, D. O. López, J. Muntasell, J. Ll. Tamarit, N. B. Chanh, and Y. Haget, *J. Chim. Phys.* **87,** 1835 (1990).
16. H. A. Rose and A. van Camp, *Anal. Chem.* **28,** 1790 (1956).
17. M. Barrio, J. Font, D. O. López, J. Muntasell, J. Ll. Tamarit, P. Negrier, and Y. Haget, *J. Phys. Chem. Solids* **55,** 1295 (1994).
18. J. Salud, Doctoral thesis, Barcelona, in preparation.
19. D. Eilerman, R. Lippman, and R, Rudman, *Acta Crystallogr. Sect. B* **39,** 263 (1983).
20. N. Doshi, M. Furman, and R. Rudman, *Acta Crystallogr. Sect. B* **29,** 143 (1973).
21. R. Zannetti, *Acta Crystallogr.* **14,** 203 (1961).
22. V. H. P. Frank, K. Krzemicki, and H. Völlenke, *Chem. Z.* **97,** 206 (1973).
23. M. Barrio, D. O. López, J. Ll. Tamarit, P. Negrier, and Y. Haget, *J. Mater. Chem.* **5,** 431 (1995).
24. J. van Braak, D. O. López, and H. A. J. Oonk, unpublished results.
25. D. Chandra, W. Ding, and R. A. Lynch, *J. Less Common Metals* **168,** 159 (1991).
26. M. Barrio, J. Font, D. O. López, J. Muntasell, J. Ll. Tamarit, P. Negrier, N. B. Chanh, and Y. Haget, *J. Phys. Chem. Solids* **54,** 171 (1993).
27. S. Urban, J. Domoslawski, and Z. Tomkowiz, *Mater. Sci.*, **IV/3,** 91 (1978).
28. J. Bouwstra, N. Brouwer, A. C. G. van Genderen, and H. A. J. Oonk, *Thermochim. Acta* **38,** 97 (1980).
29. H. A. J. Oonk, "Phase Theory." Elsevier Science, Amsterdam, 1981.
30. L. Robles-Beneyt, Doctoral thesis, Bordeaux, 1995.
31. J. S. van Duijnevldt, F. S. A. Baas, and H. A. J. Oonk, "Prophase, an MS-DOS Program for the Calculation of Binary T–X Phase Diagrams." University of Utrecht, 1988.
32. W. J. M. van der Kemp, J. G. Blok, P. R. van der Linde, H. A. J. Oonk, A. Schuijff, and M. L. Verdonk, *Thermochim. Acta* **225,** 17 (1993).
33. D. O. López, J. van Braak, J. Ll. Tamarit, and H. A. J. Oonk, *Calphad* **18,** 387 (1994).
34. J. van Braak, D. O. López, J. Salud, J. Ll. Tamarit, M. H. G. Jacobs, and H. A. J. Oonk, *J. Crystallogr. Growth*, in press.

J. Appl. Cryst. (1998). **31**, 748–757

Anisotropy of Intermolecular Interactions from the Study of the Thermal-Expansion Tensor†

J. Salud,[a] M. Barrio,[a] D. O. López,[a] J. Ll. Tamarit[a]* and X. Alcobé[b]

[a]*Departament de Física i Enginyeria Nuclear, Universitat Politècnica de Catalunya, ETSEIB, Diagonal, 647 08028 Barcelona, Catalonia, Spain, and* [b]*Serveis Científico–Tècnics, Universitat de Barcelona, Lluís Solé i Sabaris, 1-3 08028 Barcelona, Catalonia, Spain. E-mail: tamarit@fen.upc.es*

(Received 13 September 1997; accepted 1 April 1998)

Abstract

The anisotropy of the intermolecular interactions in the low-temperature ordered phases of three chemically and structurally related compounds [neopentylglycol, $(CH_3)_2C(CH_2OH)_2$, pivalic acid, $(CH_3)_3C(COOH)$, and neopentylalcohol, $(CH_3)_3C(CH_2OH)$], all of which display an orientationally disordered high-temperature phase, has been shown by means of the isobaric thermal-expansion tensor. The variation of the directions of the principal components of the thermal-expansion tensor as a function of temperature, as well as the variation of its principal coefficients, is evidence of the large differences in the intermolecular interactions for each compound; or, more precisely, between the strong intermolecular hydrogen bonds and the weak van der Waals interactions. In addition, the differences in the hydrogen-bonding schemes expected *a priori* from the molecular structures of the studied compounds have been enhanced. Finally, the volume expansivity as well as the packing coefficient have been analysed in the orientationally disordered high-temperature phase of each of the three compounds.

1. Introduction

A group of chemically and structurally related molecular compounds formed by tetrahedral molecules has been investigated by X-ray powder diffraction. The substances studied, which were neopentylglycol (NPG), $(CH_3)_2C(CH_2OH)_2$, pivalic acid (PA), $(CH_3)_3C(COOH)$, and neopentylalcohol (NPA), $(CH_3)_3C(CH_2OH)$, are known to exhibit in the solid state a phase transition from an ordered solid phase II to an orientationally disordered phase I (ODIC state) with a high enthalpy variation. For a set of similar compounds (one of them being NPG), such a high change was initially associated with the complete breakdown of the hydrogen bonds present in the low-temperature phase II on the basis of IR spectroscopy (Benson *et al.*, 1986). This suggestion, which was met with sharp criticism by a large number of authors, has now been refuted as a result of the study of the packing coefficients as well as the analysis of the Raman spectra, NMR and dielectric studies of related compounds (Barrio *et al.*, 1995, 1996; Schroetter & Bougeard, 1987; Würflinger, 1993; Granzow, 1996; Tamarit, Perez-Jubindo & de la Fuente, 1997; Tamarit, Barrio *et al.*, 1997). With respect to the ordered phase II for the substances studied in this work, we report on the anisotropy of the intermolecular interactions by means of the study of the isobaric thermal-expansion tensor in the range from 93 K up to the II-to-I phase transition of the compounds.

The isobaric thermal-expansion tensor of organic crystals has only been determined in a few cases. It is quite obvious that the crystal structure is determined jointly by different factors, such as thermal expansion, elasticity, thermodynamic properties *etc.* Nevertheless, some information can be obtained from the study of the thermal-expansion tensor. Thus, it is well known that the deformation of a structure by a change in the temperature-intensive parameter will be minimal in the directions in which the intermolecular distances are small, *i.e.* in areas of the highest atomic density. This idea was first proposed by Garnier *et al.* (1972) and Weigel *et al.* (1978). The principal coefficients of the isobaric thermal-expansion tensor are those of the weakest and strongest chemical interactions in the structure. This fact has been used to obtain information about a solid under different strains (see, for example, Chanh *et al.*, 1988, and references therein). In the case of organic compounds where the molecules are linked by hydrogen bonds, it is usual and indeed one expects to find a small expansion in directions containing such interactions (Kitaigorodsky, 1973).

With respect to the orientationally disordered high-temperature phase, the symmetry of which is face-centred cubic (f.c.c.) for the three compounds studied, and according to Neumann's principle, the directions of the principal components of the thermal-expansion tensor are parallel to the crystallographic axes and, moreover, the three principal coefficients are equal. Thus, only the isobaric volume expansivity, defined as $\alpha_V = (1/V)(\partial V/\partial T)_p$, will be reported. The analysis of this parameter as well as the packing coefficient, both as a function of temperature, enables us to determine the relative degree of the intermolecular interactions.

† Part of this work was presented at the EPDIC 1997 meeting (5th European Powder Diffraction Conference).

© 1998 International Union of Crystallography
Printed in Great Britain – all rights reserved

Table 1. *Symmetries of the ordered (II) and disordered (I) phases and transition temperatures for the substances studied*

	NPG	PA	NPA
Phase II	Monoclinic ($P2_1/n$, $Z = 4$)[(a)]	Triclinic ($P\bar{1}$, $Z = 4$)[(d)]	Triclinic ($Z = 7$)
T_{II-I} (K)	314.6[(b)]	279.8[(e)]	237.4[(g)]
Phase I	f.c.c. ($Fm3m$, $Z = 4$)[(c)]	f.c.c. ($Fm3m$, $Z = 4$)[(f)]	f.c.c. ($Z = 4$)[(h)]
T_{I-L} (K)	401.3[(b)]	308.7[(e)]	329.8[(i)]

References: (*a*) Chandra *et al.* (1993); (*b*) Barrio *et al.* (1995); (*c*) Zannetti (1961); (*d*) Longueville *et al.* (1978); (*e*) Reuter *et al.* (1997); (*f*) Namba & Oda (1952); (*g*) Suenaga *et al.* (1990); (*h*) Carpenter (1969); (*i*) Salud (1998).

This work forms part of a more general framework for studying the syncrystallization problem, which is the subject of the REALM† group. The compounds analysed in the present work are also used in our program of the study of miscibility in the ordered as well as the disordered phases of ODIC crystals.

2. Experimental

2.1. *Materials*

The substances were purchased from Aldrich Chemical Company with purities of 99.9% for NPG, 99% for PA and 99% for NPA. The well known standard procedures (Barrio *et al.*, 1995, 1996) were used to perform additional purification, the result of which was controlled by differential scanning calorimetry (Perkin-Elmer DSC-7).

2.2. *X-ray powder diffraction*

All the measurements were performed with a horizontally mounted INEL cylindrical position-sensitive detector (CPS-120) (Ballon *et al.*, 1983) equipped with a liquid-nitrogen INEL CRY950 cryostat (80–330 K). The detector, with a radius of curvature of 250 mm, was used in Debye–Scherrer geometry enabling a simultaneous recording of a powder pattern over a range of 120°(2θ). Monochromatic Cu $K\alpha_1$ radiation was selected with an asymmetric focusing incident-beam curved quartz monochromator. The generator power was set to 40 kV and 30 mA. The section of the beam was 6.3 mm (V) × 0.3 mm (H) as selected by the slit system placed just before the sample. The powder samples were introduced in 0.5 mm Lindemann capillaries which rotate during the experiment to improve averaging of the crystallites. The design of the cryostat was modified in order to measure the temperature by means of a Pt 100 Ω device in the sample chamber (which contains He gas as heat exchanger) and not in the vacuum chamber as in the original design.

External calibration using the cubic phase $Na_2Ca_3Al_2F_{14}$ (NAC), following recommendations (Deniard *et al.*, 1991; Evain *et al.*, 1993), was used to convert the measured channels to °(2θ) by means of cubic spline fittings. The lack of peaks for $2\theta > 60°$ for the materials studied enabled us to work with only 20 points of calibration in the 0–60°(2θ) range. *DIFFRACTINEL* software was used for the calibration and for the peak position determination after Gaussian fittings.

A set of powder diffractograms was obtained for at least every 20 K step in the temperature range of the ordered solid phases II (from 93 K to the II-to-I phase transitions) and for every 5 K step in the temperature range of the orientationally disordered phases I (from the II-to-I transitions to the melting point for PA and NPA, and to 323 K for NPG). The acquisition times were 60 min for the patterns of phase II and 30 min for those of phase I. The slew rate was 1 K min^{-1} with a stabilization time of 10 min at each temperature before data acquisition.

Additional data reported previously (Barrio *et al.*, 1995, 1996) for the lattice parameters in the high-temperature range of the ODIC state were also used for NPG.

3. Data analysis

For indexing purposes for the patterns collected, we have calculated the theoretical pattern from the reported structure in the cases of NPG (Chandra *et al.*, 1993; Strauss *et al.*, 1996) and PA (Longueville, 1987) from the *FULLPROF* program (Rodriguez-Carvajal, 1990). For the NPA compound we used the program *DICVOL*91 (Louer & Boultif, 1992) to determine the unknown symmetry of phase II of NPA. After indexing the patterns, lattice parameters were refined by means of the *AFMAIL* (Rodriguez-Carvajal, 1985) program at each temperature. The crystallographic properties and transition temperatures for the substances are summarized in Table 1.

In order to determine the thermal-expansion tensor of the ordered phase II for each compound, the refined lattice parameters were fitted as a function of the temperature using a standard least-squares method for each parameter. The agreement between the calculated and experimental values has been estimated with the help of the reliability factor defined as $R = \sum(y_0 - y_c)^2 / \sum y_c^2$, where y_0 and y_c are the measured

† Réseau Européen d'Alliages Moléculaires (General Coordinator Y. Haget).

Table 2. *Lattice constants corresponding to ordered solid phases were fitted to the polynomial equation* $p = p_0 + p_1T + p_2T^2$ *(T in K) where p is the lattice constant and R the reliability factor between the measured and calculated unit-cell parameters*

Compound	p	p_0	$p_1 \times 10^3$	$p_2 \times 10^5$	$R \times 10^5$
NPG	a	5.978 (2)	0.73 (7)		27
	b	10.507 (5)	1.15 (5)	0.05 (1)	16
	c	10.764 (8)	−0.21 (8)	0.16 (2)	24
	β	113.86 (5)	−3.6 (5)	0.41 (12)	14
PA	a	9.229 (19)	−0.60 (2)	0.45 (6)	55
	b	10.709 (8)	−0.11 (4)		69
	c	6.339 (5)	1.08 (2)		72
	α	102.4 (2)	6.0 (3)	−4.5 (7)	63
	β	95.09 (9)	5.0 (5)		90
	γ	104.60 (2)	7.0 (1)		21
NPA	a	10.065 (5)	1.07 (3)		30
	b	10.144 (26)	1.5 (3)	−0.14 (10)	37
	c	11.030 (17)	1.6 (1)		98
	α	89.92 (7)	0.8 (4)		51
	β	99.6 (2)	−5.0 (3)	2.2 (1.0)	37
	γ	106.8 (3)	6.8 (4)	−2.6 (1.4)	47

and calculated lattice constants, respectively, and the sum extends over all the experimental values. The polynomial coefficients corresponding to the lattice parameters are given in Table 2 together with the reliability factor.

The cell deformation dU due to a small temperature variation dT is expressed by a second-rank tensor (α_{ij}), $dU_{ij} = \alpha_{ij}dT$, the coefficients of the thermal-expansion tensor being expressed in K^{-1}. At a given temperature, knowledge of the principal coefficients and of the direction of the principal axes of the tensor allows the determination of the highest and weakest directions of the deformations related to the directions of the corresponding intermolecular interactions (Garnier *et al.*, 1972). Such directions will be referred to in this paper as 'soft' and 'hard' directions, respectively. The procedure and the method have been published elsewhere (Chanh *et al.*, 1988) and the program *DEFORM* (Filhol *et al.*, 1987) was used for the calculation of the tensor. The number of patterns collected in the low-temperature ordered phases was 12 for NPG and NPA, and 11 for PA.

In relation to the orientationally disordered high-temperature phase I, the isobaric volume expansivity was directly determined from the assumed linear dependence of the lattice parameter with the temperature. Such a linear dependence was assumed because of the large error on the lattice parameters determined. This error was produced by the use of only two low-order reflections appearing in the patterns, which reveal a large Debye factor as a consequence of the highly disordered structures. The calculation of the packing coefficient, defined as $\kappa = V_m/V_Z$, V_m being the molecular volume and V_Z the volume occupied by a molecule in the lattice, requires evaluation of the molecular volume, V_m, while V_Z is obtained experimentally. A simplified model was used to determine V_m based on the consideration of rigid molecules and assuming that the atoms of these molecules are maintained at a constant distance. In spite of these simple assumptions, this model has been proved to be valid (Barrio *et al.*, 1996; Tamarit, Barrio *et al.*, 1997). The van der Waals radii and interatomic chemical bonds used have been reported previously (Tamarit, Barrio *et al.*, 1997).

4. Results and discussion

4.1. *Low-temperature ordered phases*

4.1.1. *NPG.* The low-temperature ordered phase II of NPG was first determined (Zannetti, 1961) as monoclinic $P2_1/n$. More recently, two independent studies, both at room temperature (Chandra *et al.*, 1993; Strauss *et al.*, 1996), reporting on the structure have been published. The lattice parameters have been determined in the range 93–313 K, *i.e.* practically in the whole temperature domain of phase II [stable from 313 to 60 K, where a phase transition to a phase III has been reported (Suenaga *et al.*, 1990)]. The polynomial equations accounting for the lattice-parameter variations are listed in Table 2. Such polynomial equations are plotted together with the experimentally determined lattice parameters in Fig. 1.

The tensor of a monoclinic lattice is completely defined by the principal coefficients, α_1, α_2 and α_3, for an angle φ between the direction of one of the principal directions (α_3 in the present case) and the crystallographic axis a, the α_1 axis being coincident with the binary b axis of the crystal. Fig. 2 depicts the variation of the α_1, α_2 and α_3 coefficients and the φ angle with temperature for phase II of NPG.

As can be inferred from Fig. 2, the intermolecular interactions joining the tetrahedral molecules of NPG *via* O–H bonds are highly anisotropic. The principal axes of the tensor corresponding to the lowest values of the principal coefficients (α_2 and α_3), *i.e.* the hard directions, are located in the (010) crystallographic plane. That means that the O–H bonds have to form chains inside this plane and, moreover, that two kinds of hydrogen bonds with slight differences are present (Chandra *et al.*, 1993; Strauss *et al.*, 1996). Such differences in the interactions produce slight differences in the hydrogen-bond distances that have been reported in previous studies of the structures: 2.686 (4) and 2.720 (4) Å (Chandra *et al.*, 1993) and 2.68 (1) and 2.73 (1) Å (Strauss *et al.*, 1996). The change of the angle between the α_3 axis and the crystallographic a direction of about 40° in the whole temperature range studied could be associated with a shift in the hydrogen-bond directions, but no structural information at low-temperature is available to verify this assumption.

In Fig. 3 we plot the *ac* crystallographic plane (calculated from Chandra *et al.*, 1993) showing the chains linking the molecules, together with the principal axes (α_2 and α_3) of the tensor obtained. The value of the principal coefficient α_1 indicates that it corresponds to the weakest intermolecular interaction (soft direction) as a consequence of the existence of weak van der Waals interactions in this direction.

Finally, Fig. 4 shows a three-dimensional plot of the isobaric thermal-expansion tensor at different temperatures in the frame of the principal axes α_1, α_2 and α_3, together with the direction of the crystallographic axes. As can be seen from Figs. 2 and 4 the deformation decreases with the temperature, even producing a contraction in the principal direction α_3. Moreover, these figures clearly show that with a decrease in temperature the principal axis α_3 (corresponding to the lowest deformation, *i.e.* the highest intermolecular interaction) is further away from the *a* crystallographic direction

4.1.2. *PA*. Below 280 K, PA exhibits a solid phase II, the symmetry of which has been found to be $P\bar{1}$ (Longueville *et al.*, 1978). Between 280 K and the melting temperature (309 K) PA displays an orientationally disordered f.c.c. phase, probably *Fm3m* (Namba & Oda, 1952). In previous studies (Kondo & Oda, 1954; Kondo, 1965), it was proposed that this disordered phase is formed by nonpolar dimer units having disordered orientation along the 12 [110] directions of the cubic lattice. Such an idea has been largely proved (Suenaga *et al.*, 1990; Longueville *et al.*, 1978). In contrast, there is much debate as to the extent of the hydrogen bonding in the low-temperature ordered phase. The complete structure has been obtained from Longueville (1987), the general trends being partially published (Longueville *et al.*, 1978). In these studies, the authors assert the existence of dimers parallel to the (110) planes of the triclinic lattice: 'Two dimers, one above each other along the *c* axis, are nearly orthogonal'. However, the peculiarities observed by many spectroscopic techniques

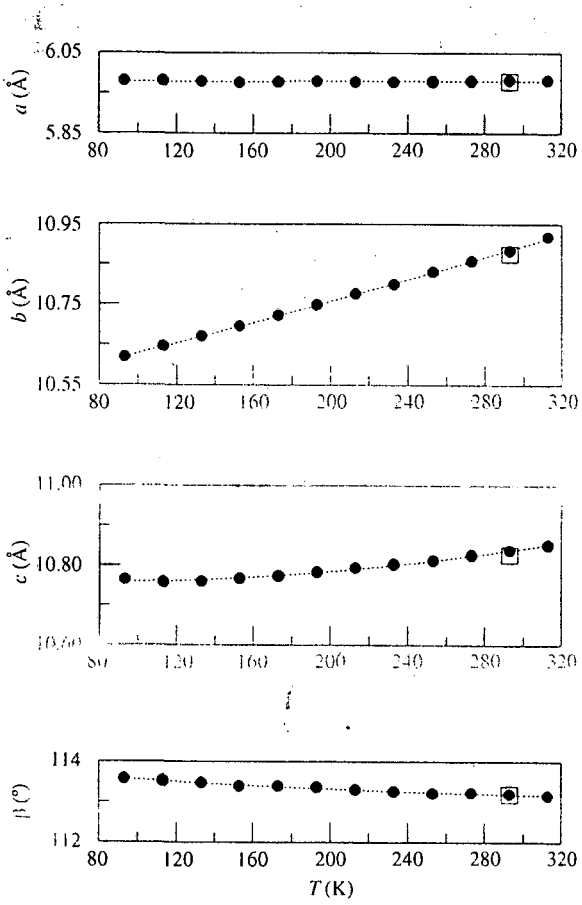

Fig. 1. Lattice parameters for phase II of NPG as a function of temperature. □ From Chandra *et al.* (1993).

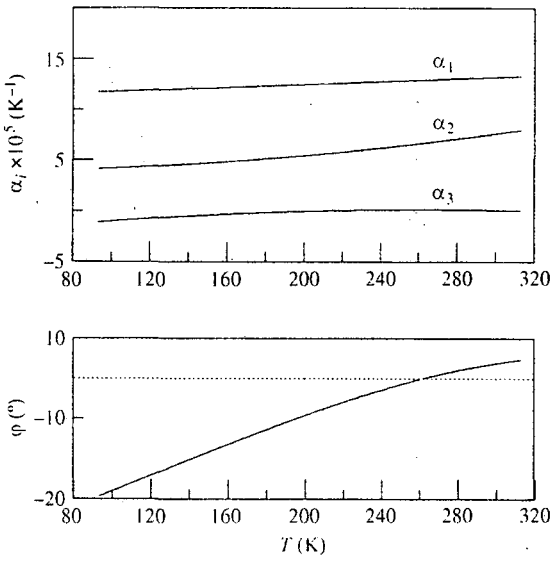

Fig. 2. The α_1, α_2 and α_3 coefficients and φ angle as a function of temperature for NPG.

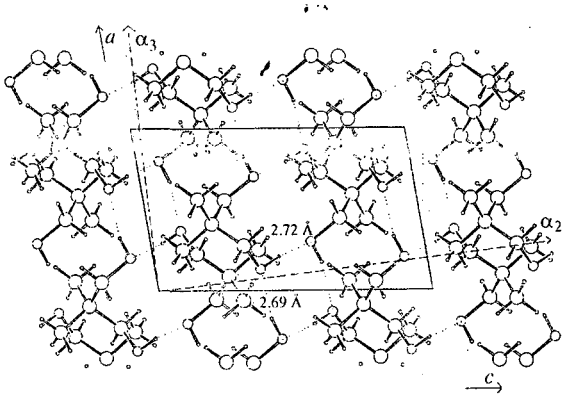

Fig. 3. The *ac* crystallographic plane of the monoclinic phase II of NPG calculated from Chandra *et al.* (1993) at 293 K.

have so far not been satisfactorily accounted for. At this point, several reports have pointed out the possibility of the existence of cyclic dimers distorted to the extent that they form open dimers and/or polymers in the ordered phase of pivalic acid (Hasebe *et al.*, 1981; Aksnes *et al.*, 1984; Kimtys *et al.*, 1992).

The thermal-expansion tensor in the ordered phase has been determined from 93 K up to the II-to-I transition (280 K) through measurement of the lattice parameters (see Fig. 5). Because of the low symmetry of this phase (triclinic) the principal directions of the tensor are not coincident with the crystallographic axes. Fig. 6 depicts the evolution of the principal coefficients of the thermal-expansion tensor as a function of temperature. In the whole of the temperature range studied of phase II the α_1 direction corresponds to a soft direction which, as can be seen from Fig. 7 (where a three-dimensional plot of the thermal-expansion tensor is presented), is relatively close to the [001] crystallographic direction. This experimental result indicates that in such a direction no intermolecular hydrogen bonds are present. This evidence agrees with the structure proposed by Longueville *et al.* (1978) for which the dimers are nearly parallel to the (110) plane. Fig. 8 depicts the (00*l*) crystallographic plane showing the almost orthogonal dimers along the *c* axis at 223 K.

The other two directions α_2 and α_3 display relatively low values of the principal coefficients in the lower temperature range studied, thus corresponding to hard directions, *i.e.* the $\alpha_2\alpha_3$ plane contains the highest intermolecular interactions. From the principal directions of the tensor (see Fig. 7) we can see that the hard plane is close to the (00*l*) crystallographic plane. Such results agree again with the structure proposed by Longueville and co-workers. Nevertheless, it must be pointed out that with an increase in temperature the α_2 direction becomes softer. This may be associated with a possible twist of the two molecules of the asymmetric unit along the *b* crystallographic axis. In this situation, the atomic density in the α_2 direction (close to **a**) would be diminished and then thermal expansion would be increased, producing the opposite effect in the α_3

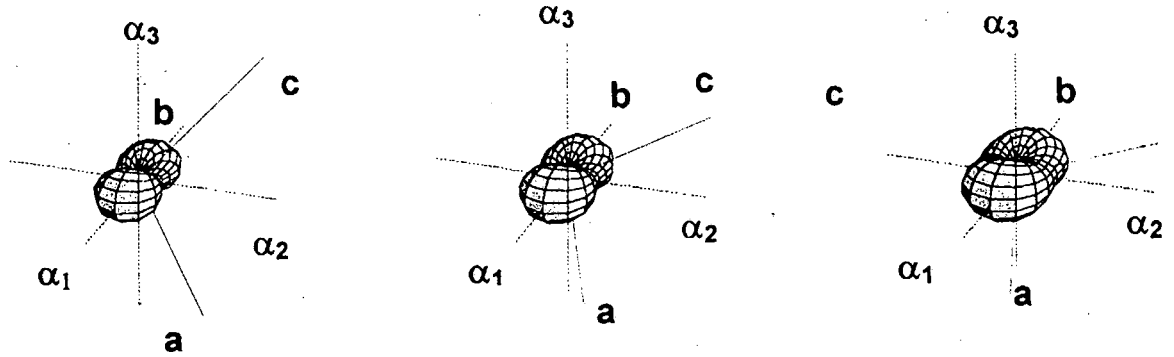

Fig. 4. The thermal-expansion tensor of phase II of NPG at several temperatures (T = 113, 213, 293 K from left to right) in the frame of the principal directions α_1, α_2 and α_3 (dotted line) together with the crystallographic axes *a*, *b* and *c* (continuous line). The full length of the α_i axis corresponds to 5×10^{-4} K^{-1}.

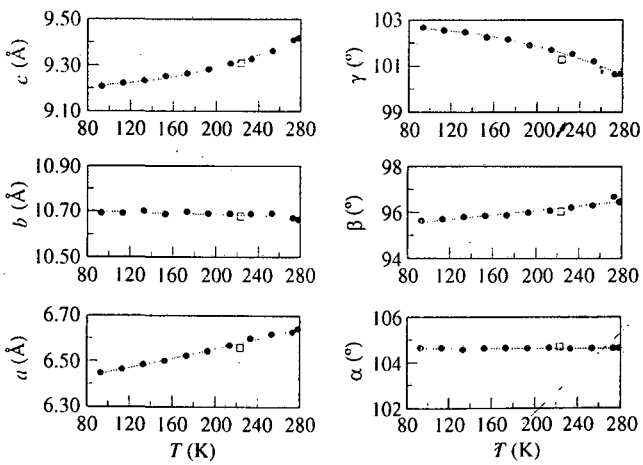

Fig. 5. Lattice parameters for phase II of PA as a function of temperature. □ From Longueville *et al.* (1978).

direction, which would be compatible with the hardening of this direction represented in Fig. 6. The work of Aksnes *et al.* (1984) reveals the existence of new bands in the IR spectra of PA when the temperature approaches the solid-to-plastic phase transition; this is assigned to a twisting of the carboxyl groups. A subsequent NMR study (Kimtys *et al.*, 1992) has established a model based on the occurrence of a second-order phase transition within the dimer unit which is caused by a change of its average symmetry in the temperature range 250–280 K. Such a temperature-dependent structural anomaly should be investigated by resolving the structure near the transition temperature from the brittle to plastic phases. In both cases, the conclusion corresponds to a continuous and slow change in the hydrogen-bond interactions when the temperature approaches the order–disorder transition.

4.1.3. *NPA*. NPA is known to occur in two different solid phases (Suenaga *et al.*, 1990). The low-temperature ordered phase II is stable up to 237.4 K. The orientationally disordered high-temperature phase, the structure of which is f.c.c. [probably *Fm3m* (Carpenter, 1969)], is stable up to the melting point at about 330 K.

The hitherto unknown symmetry of the low-temperature phase II has been determined by means of X-ray powder diffraction following the procedure described in §3 of this work. This symmetry has been determined to be triclinic with lattice parameters a = 10.304 (10), b = 10.418 (9), c = 11.398 (12) Å, α = 90.14 (6), β = 99.51 (3) and γ = 107.08 (1)° (Z = 7) at 233.2 K. From the variation of the lattice parameters with the temperature (Fig. 9), the thermal-expansion tensor, whose principal coefficients are depicted in Fig. 10 *versus* temperature, has been determined. In the case

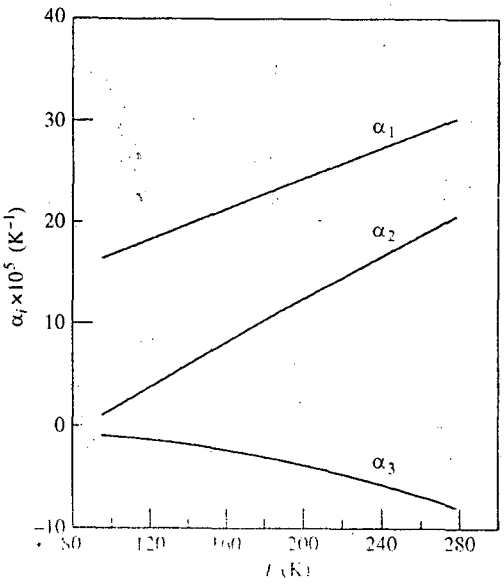

Fig. 6. The α_1, α_2 and α_3 coefficients as a function of temperature for PA.

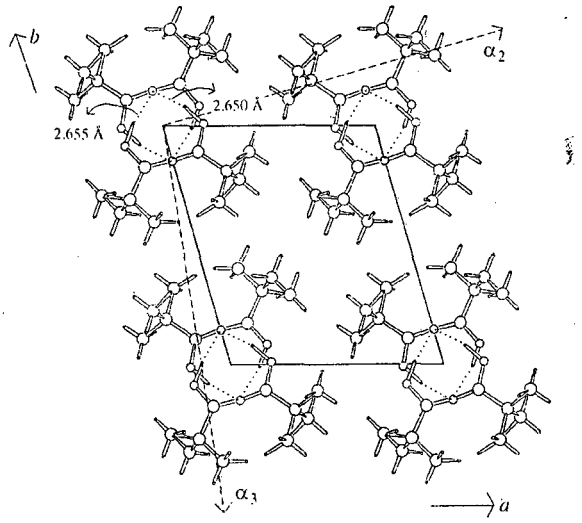

Fig. 8. The (00l) crystallographic plane of the triclinic phase II of PA calculated from Longueville (1987) at 223 K. One dimer unit is at z = 0 (or z = 1) and the other at z = 0.5.

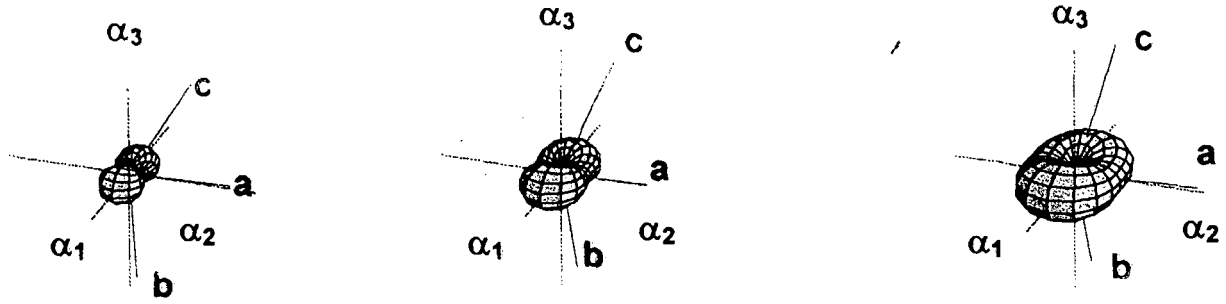

Fig. 7. The thermal-expansion tensor of phase II of PA at several temperatures (T = 133, 193, 273 K from left to right) in the frame of the principal directions α_1, α_2 and α_3 (dotted line) together with the crystallographic axes a, b and c (continuous line). The full length of the α_i axis corresponds to 10^{-3} K^{-1}.

of NPA, the principal directions of the thermal-expansion tensor all have components in the three crystallographic directions, making a straightforward interpretation on the basis of the unknown structure difficult. At low temperature, the three principal coefficients reach similar values (about 10^{-4} K^{-1}) and, thus, the thermal-expansion tensor is rather isotropic. Increasing the temperature from about 140 K, the principal coefficients move away (increasing the anisotropy of the deformation). In the high-temperature region of phase II it is quite obvious that the α_1 direction becomes soft, while the $\alpha_2\alpha_3$ plane remains hard (see Fig. 11). In an early work (Faucher *et al.*, 1966) the loss modulus of the solid phase II was recorded as a function of temperature by means of a torsion pendulum. The authors indicated the existence of a 'secondary' transition at about 150 K, which with the help of the NMR measurements was interpreted as an increase of the

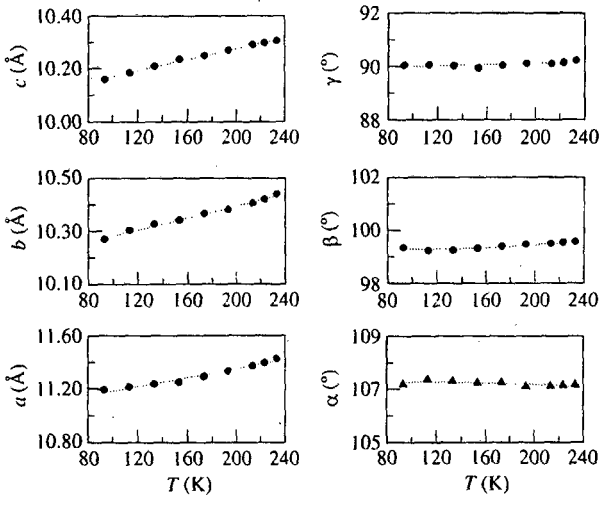

Fig. 9. Lattice parameters for phase II of NPA as a function of temperature.

small segment mobility in polymers or the onset of

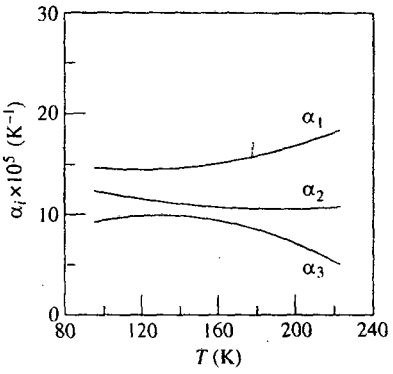

Fig. 10. The α_1, α_2 and α_3 coefficients as a function of temperature for NPA.

limited molecular motion in a monomeric material. Nevertheless, the accurate c_p measurements from Suenaga *et al.* (1990) do not display any thermal anomaly in the temperature range from 12.7 K to the II-to-I phase transition at 237.4 K. From the present work, we can see that only a slow softening in the α_1 direction, close to the *c* crystallographic direction (see Fig. 11), is present. On the other hand, variation of the volume thermal expansivity (see §4.1.4) has no relevant effect. However, it must be pointed out that in order to detect a structural phase transition (without associated thermal effects) the X-ray diffraction measurements should be performed with very narrow temperature steps and, if possible, on a single crystal in order to evidence weak superlattice reflections.

In spite of the limited structural information to explain the thermal-expansion tensor, we can reasonably conclude that, as in the previous case of PA, the intermolecular interactions by hydrogen bonds in NPA take place in the $\alpha_2\alpha_3$ plane of the deformation space (close to the *ab* crystallographic plane).

4.1.4. *Isobaric thermal expansivity in the low-temperature phases of NPG, PA and NPA: a comparative analysis.* Fig. 12 shows the variation of the volume expansivity (α_V) of the compounds studied with temperature in the ordered as well as in the orientationally disordered phases. For phase II, the lowest value of the volume expansivity corresponds to NPG, in agreement with the previous finding of a very hard plane in the structure of its phase II.

For PA we can see a continuous and slow increase in the α_V parameter which is due to the discussed change in the hydrogen-bond interactions when the temperature increases. The α_V value for NPA is higher than those corresponding to NPG and PA, except at temperatures close to the transition, where the hydrogen bonds remain in a plane network unlike PA but similar to NPG. At this point it should be emphasized that any analysis of the volume expansivity neglects the details corresponding to the specific intermolecular interactions and thus all the details about a possible anisotropy. To account for this, an asphérism index A has been defined as

$$A = (2/3)[1 - (3\beta/\alpha_V^2)]^{1/2}$$

where $\beta = \alpha_1\alpha_2 + \alpha_2\alpha_3 + \alpha_3\alpha_1$ (Weigel *et al.*, 1978). This coefficient reaches the zero value when the thermal-expansion tensor is isotropic. Fig. 13, which shows the behaviour of the A index as a function of temperature in the ordered phases, illustrates the anisotropy peculiarities described earlier. The evolution of the A index for NPA reaches lower values at about 100 K below the II-to-I order–disorder phase transition (*i.e.* at about 140 K), although it does not vary greatly with temperature. In a previous work, where the thermal expansion was determined for a considerable number of

inorganic solids (Weigel *et al.*, 1978), the strong anomalies of the aspherism index were assigned to the possibility of the existence of a transition associated with an order parameter. For such a transition, the volume expansivity is due to the anharmonicity of the thermal vibrations and to the deformation of the lattice as a consequence of the phase transition, the latter contribution being larger than the former. In the case of the NPA compound the lattice symmetry does not change at 140 K (there are no relevant changes in the patterns collected). Therefore, the possible phase transition should have a second-order character. This possibility seems to be rather limited taking into account the continuous evolution of both the volume expansivity and c_p values with temperature at the considered domain.

In the light of these considerations and because of the lack of more structural information, the existence of a phase transition is discarded at present and it is concluded that these slight changes concern certain modifications of the molecular motion.

4.2. *High-temperature orientationally disordered phases*

The polynomial equations accounting for the lattice parameter of the orientationally disordered phases are given in Table 3. The variation of the volume expansivity for the orientationally disordered phases with temperature is depicted in Fig. 12. The figure shows that the packing in such a phase is controlled by means of the intermolecular interactions *via* hydrogen bonds. The lowest volume expansivity corresponds once more to the NPG compound, for which the now dynamic and isotropically distributed hydrogen bonds remain in the disordered phase. A very recent dielectric relaxation study on phase I of NPG (Tamarit, Pérez-Jubindo & de la Fuente, 1997) has proved their existence throughout the determination of a high activation enthalpy for the molecular tumbling and a relatively low relaxation frequency as compared with other ODICs without such an intermolecular interaction. A similar situation was found in the disordered phase of NPA (Kreul *et al.*, 1992), the interaction being lower than in the previous case of NPG.

A different situation appears for phase I of PA. With regard to the molecular structure of PA, the possibility of the formation of hydrogen bonds should be very close to that of the NPA compound. However, the volume expansivity for PA reaches high values whatever the temperature. The interpretation of this experimental fact is quite obvious taking into account the well established formation of dimers in the disordered phase, the behaviour of which is controlled by van der Waals weak interactions between dimer units. Moreover, an NMR study under pressure (Hasebe *et al.*, 1981) concluded that the volume required for the molecular tumbling in this disordered phase of PA is several times

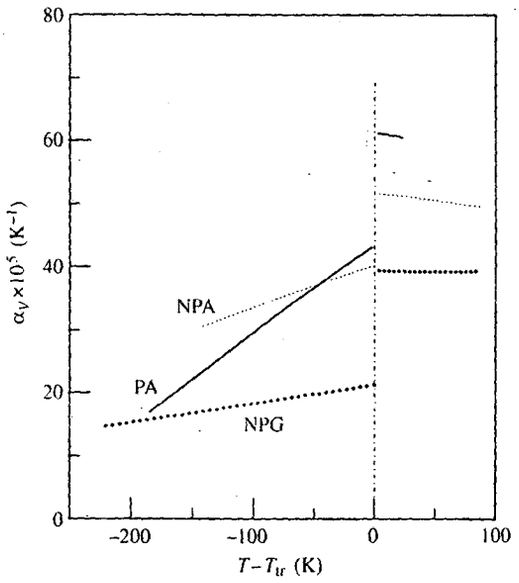

Fig. 12. The volume expansivity (α_V) as a function of temperature for NPG (dotted line), PA (continuous line) and NPA (dashed line).

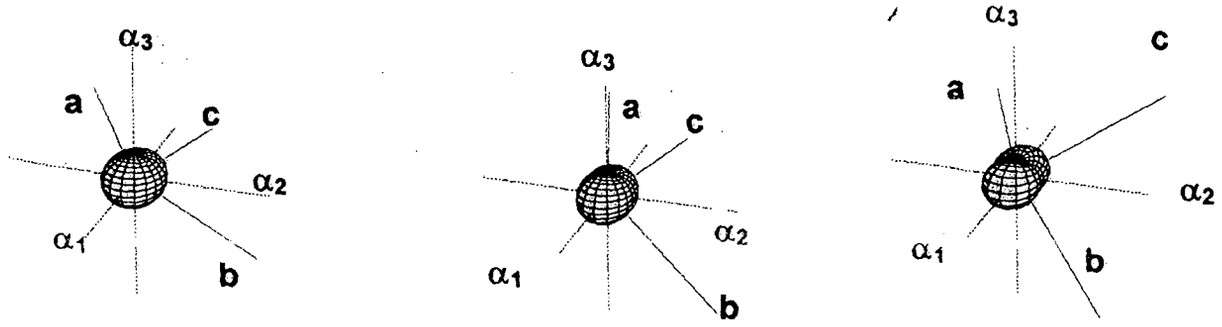

Fig. 11. The thermal-expansion tensor of phase II of NPA at several temperatures (T = 113, 153, 213 K from left to right) in the frame of the principal directions α_1, α_2 and α_3 (dotted line) together with the crystallographic axes a, b and c (continuous line). The full length of the α_i axis corresponds to 10^{-3} K^{-1}.

Table 3. *The lattice parameter of the f.c.c. orientationally disordered phase was fitted to the polynomial equation* $a = p_0 + p_1 T$ *(T in K) where p is the lattice constant and R the reliability factor between the measured and calculated unit-cell parameters*

Compound	p_0	$p_1 \times 10^3$	$R \times 10^5$
NPG	8.444 (23)	1.16 (7)	89
PA	8.347 (38)	1.80 (13)	18
NPA	8.364 (86)	1.5 (3)	32

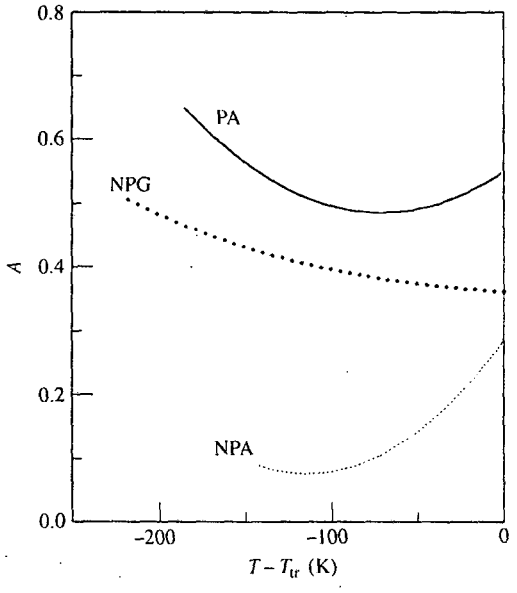

Fig. 13. The aspherism index (A) as a function of temperature for phases II of NPG (dotted line), PA (continuous line) and NPA (dashed line).

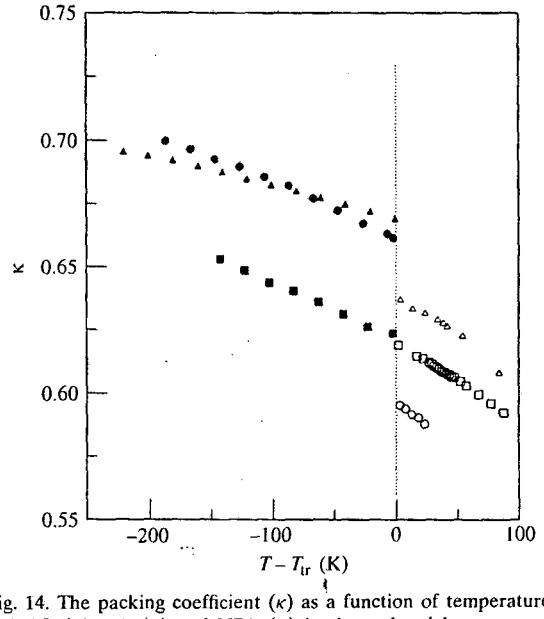

Fig. 14. The packing coefficient (κ) as a function of temperature for NPG (△), PA (○) and NPA (□) in the ordered low-temperature phases (filled symbols) and in the orientationally disordered high-temperature phases (empty symbols).

higher than that of related compounds, indicating the existence of units formed by two molecules. To corroborate this, the packing coefficient was calculated for the three compounds as a function of the temperature.

Fig. 14, which shows the variation of the packing coefficient with temperature in the whole temperature range studied, confirms the previous findings. The lowest packing in the ODIC state corresponds to that of PA according to the weak van der Waals interaction between dimer units. The highest packing is found to be for NPG showing that hydrogen bonds are still active in the disordered phase. Similar behaviour can be inferred for the disordered phase of NPA, which shows a lower value of the packing than the corresponding NPG according to the diminution of the available number of CH_2OH groups. The small change in the packing coefficient at the order–disorder phase transition of NPA should also be noted. This effect would mean that the dynamic character of the hydrogen bonds in phase I (isotropically distributed in this case) should not be very different from that previously established in phase II (anisotropically distributed in this phase and, particularly, in a plane) near the transition point.

The authors wish to thank the referees for their valuable comments and particularly for providing us with the unpublished structural data for one of the substances. We acknowledge the financial support of the DGICYT (grant PB95-0032).

References

Aksnes, D. W., Kimtys, L. K., Balevicius, V. J. & Balevicius, M. Z. (1984). *Acta Chem. Scand. Ser. A*, **38**, 163–168.

Ballon, J., Comparat, V. & Pouxe, J. (1983). *Nucl. Instrum. Methods*, **217**, 213–216.

Barrio, M., López, D. O., Tamarit, J. Ll., Negrier, P. & Haget, Y. (1995). *J. Mater. Chem.* **5**, 431–439.

Barrio, M., López, D. O., Tamarit, J. Ll., Negrier, P. & Haget, Y. (1996). *J. Solid State Chem.* **124**, 29–38.

Benson, D. K., Barrows, R. W. & Webb, J. D. (1986). *Sol. Energy Mater.* **13**, 133.

Carpenter, G. B. (1969). *Acta Cryst.* B**25**, 163.

Chandra, D., Day, C. S. & Barret, C. S. (1993). *Powder Diffr.* **8**, 109–117.

Chanh, N. B., Clastre, J., Gaultier, J., Haget, Y., Meresse, A., Lajzerowicz, J., Filhol, A. & Thomas, M. (1988). *J. Appl. Cryst.* **21**, 10.

Deniard, P., Evain, M., Barbet, J. M. & Brec, R. (1991). *Mater. Sci. Forum*, **79–82**, 363–370.

Evain, M., Deniard, P., Jouanneaux, A. & Brec, R. (1993). *J. Appl. Cryst.* **26**, 563–569.

Faucher, J. A., Graham, J. D., Koleste, J. V., Santee, E. R. & Walter, E. R. (1966). *J. Phys. Chem.* **70**, 3738–3740.

Filhol, A., Lajzerowicz, J. & Thomas, M. (1987). *DEFORM*. Unpublished software.

Garnier, P., Calvarin, G. & Weigel, D. (1972). *J. Chim. Phys. Phys.-Chim. Biol.* **11–12**, 1711–1718.

Granzow, B. (1996). *J. Mol. Struct.* **381**, 127–131.

Hasebe, T., Soda, G. & Chihara, H. (1981). *Bull. Chem. Soc. Jpn*, **54**, 2583–2586.
Kimtys, L. K., Balevicius, V. J. & Aksnes, D. W. (1992). *J. Mol. Struct.* **270**, 161–171.
Kitaigorodsky, A. I. (1973). In *Molecular Crystals and Molecules, Physical Chemistry Series* No. 29, edited by E. M. Loebl. New York: Academic Press.
Kondo, S. (1965). *Bull. Chem. Soc. Jpn.*, **38**, 27.
Kondo, S. & Oda, T. (1954). *Bull. Chem. Soc. Jpn.*, **27**, 567–570.
Kreul, H. G., Waldinger, R. & Würflinger, A. (1992). *Z. Naturforsch. Teil A*, **47**, 1127–1134.
Longueville, W. (1987). PhD thesis, University of Lille, France.
Longueville, W., Fontaine, H., Baert, F. & Odou, G. (1978). *Acta Cryst.* A**34**, S188.
Louer, D. & Boultif, A. (1992). *DICVOL*91 program. Laboratoire de Cristallochemie, Université de Rennes I, France.
Namba, H. & Oda, T. (1952). *Bull. Chem. Soc. Jpn*, **25**, 225–226.
Reuter, J., Büsing, D., Tamarit, J. Ll. & Würflinger, A. (1997). *J. Mater. Chem.* 7, 41–46.
Rodriguez-Carvajal, J. (1985). *AFMAIL*. Laboratoire Leon Brillouin, CEA-CNRS, France.
Rodriguez-Carvajal, J. (1990). *FULLPROF* version 3.0.0, unpublished software. Laboratoire Leon Brillouin, CEA-CNRS, France.
Salud, J. (1998). PhD thesis (in preparation), Polytechnical University of Barcelona, Spain.
Schroetter, S. & Bougeard, D. (1987). *Ber. Bunsenges. Phys. Chem.* **91**, 1217–1221.
Strauss, R., Braun, S., Dou, S., Fuess, H. & Weiss, A. (1996). *Z. Naturforsch. Teil A*, **51**, 871–881.
Suenaga, K., Kanae, R., Matsuo, T. & Suga, H. (1990). In *Proc. 11th IUPAC Conf.*, Como, Italy.
Tamarit, J. Ll., Barrio, M., López, D. O. & Haget, Y. (1997). *J. Appl. Cryst.* **30**, 118–122.
Tamarit, J. Ll., Perez-Jubindo, M. A. & de la Fuente, M. R. (1997). *J. Phys. Condens. Matter*, **9**, 5469–5478.
Weigel, D., Beguemsi, T., Garnier, P. & Gerad, J. F. (1978). *J. Solid State Chem.* **23**, 241–251.
Würflinger, A. (1993). *Int. Rev. Phys. Chem.* **12**, 89–121.
Zannetti, R. (1961). *Acta Cryst.* **14**, 203–204.